Blitzen

Final Proposal

Undergraduate Design Team
University of Maryland, College Park

39th Annual Vertical Flight Society Student Design Competition

Sponsored by Bell

Alfred Gessow Rotorcraft Center
Department of Aerospace Engineering
University of Maryland
College Park, MD, 20740

Vivek Uppoor
Undergraduate Student (Team Lead/Aerodynamics)
vvuppoor@umd.edu

Sam Allgaier
Undergraduate Student (CAD)
smallgaier25@gmail.com

Sang Kim
Undergraduate Student (Batteries)
sakim98.mark@gmail.com

Sandra Crenshaw
Undergraduate Student (CAD)
screnshl@umd.edu

Eva Alexandrova
Undergraduate Student (Aerodynamics)
ealexan7@umd.edu

Brad Reamy
Undergraduate Student (Propulsion)
brad.reamy4@gmail.com

Roshni Patel
Undergraduate Student (Structures)
roshnijp21@gmail.com

Dr. Vengalattore Nagaraj
Research Scientist
vnagaraj@umd.edu

David Umansky
Undergraduate Student (Structures)
dumansky@umd.edu

Dr. Inderjit Chopra
Alfred Gessow Professor and Distinguished University
Professor, Director of AGRC
chopra@umd.edu

Andrew Giorgi
Undergraduate Student (Propulsion)
afgiorgi53@gmail.com

Dr. James Baeder
Samuel P. Langley Professor
baeder@umd.edu

Isaac Rose
Undergraduate Student (Rotor Design)
isaac.rose245@gmail.com

Students will receive credits for ENAE482 (Aeronautical Systems Design) for their contributions.

Alfred Gessow Rotorcraft Center
Department of Aerospace Engineering
University of Maryland
College Park, MD, 20740

To the Vertical Flight Society:

The members of the University of Maryland Undergraduate Student Design Team hereby grant full permission to distribute the enclosed Executive Summary and Final Proposal for the 39th Annual Design Competition as they see fit.

Regards,

The UMD Undergraduate Design Team

Acknowledgements

The University of Maryland's undergraduate team wishes to acknowledge the support of the following people for their invaluable insight, guidance, time, and support throughout the design process.

University of Maryland Faculty and Staff

- *Dr. Vengalattore Nagaraj* - Research Scientist, Department of Aerospace Engineering
- *Dr. James Baeder* - Samuel P. Langley Professor, Department of Aerospace Engineering
- *Dr. Inderjit Chopra* - Alfred Gessow Professor and Distinguished University Professor, Director of Alfred Gessow Rotorcraft Center, Department of Aerospace Engineering
- *Fred Tsai* - Aerospace Engineering Graduate Student, AGRC
- *CDR Spencer Fishman, USN* - Aerospace Engineering Graduate Student, AGRC

Industry Professionals

- *Dr. Andreas Bernhard* - Sikorsky
- *Andrew Lent* - Airgility

External

- *Dr. Ananth Sridharan*

Contents

List of Figures

List of Tables

Nomenclature

English Symbols

A_{MR}	Area of the Main Rotor
C_d	Airfoil Drag Coefficient
C_{D0}	Fuselage Zero Lift Drag Coefficient
C_{Dv}	Vertical Drag Coefficient
C_f	Skin Friction Coefficient
C_p	Power Coefficient
C_{pi}	Induced Power Coefficient
C_{po}	Profile Power Coefficient
C_{pp}	Parasitic Power Coefficient
C_T	Thrust Coefficient
f	Effective Flat Plate Area
FM	Figure of Merit
IF	Interference Factor
L/D	Lift over Drag Ratio for Main Rotor
L/D_e	Lift over Effective Drag Ratio
N_b	Number of Blades
N_{gear}	Gear Tooth Count
n_{crit}	n criterion
P_{MR}	Main Rotor Power
P_{TR}	Tail Rotor/Propeller Power
R	Rotor Radius
$R.R.$	Gear Reduction Ratio
S_{ref}	Reference Area
S_{wet}	Wetted Area
v_{cruise}	Cruise Velocity
v_{tip}	Rotor Tip Speed
$W_{payload}$	Payload Weight

Greek Symbols

α	Angle of Attack
μ	Rotor Advance Ratio
μ_f	Friction Coefficient
σ	Rotor Solidity

Abbreviations

AR	Aspect Ratio
AGL	Above Ground Level
DL	Disk Loading
$eVTOL$	Electric Vertical Takeoff and Landing
$GTOW$	Gross Takeoff Weight
$HIGE$	Hover in Ground Effect
$HOGE$	Hover out of Ground Effect
IFR	Instrument Flight Rules
ISA	International Standard Atmosphere
MR	Main Rotor
OMI	One Motor Inoperative
PRM	Passengers with Reduced Mobility
RFP	Request for Proposal
VFR	Visual Flight Rules

I. Introduction

The Vertical Flight Society's 39th Annual Student Design Competition, sponsored by Bell Helicopters in 2021-2022, tasks teams to design an Electric Vertical Takeoff and Landing (eVTOL) urban air taxi capable of accommodating persons with reduced mobility and other disabilities. Specifically, the final product should be able to transport two to four passengers within an urban environment safely, comfortably, and promptly while solely using electric power. People seeking rapid and comfortable taxi services are currently limited to ground transportation options. The goal is to create an eVTOL with superior performance over existing electric powered rotorcraft while having a reconfigurable interior design to accommodate people with disabilities in addition to fully mobile passengers.

In response to this year's RFP, the University of Maryland's undergraduate design team has developed the "Blitzen". Blitzen is a single-pilot lift and thrust compounding single main rotor helicopter capable of transporting two people with disabilities or four fully mobile passengers. It can fly for a distance of 160.9 km (100 miles) within an urban environment quickly, safely, and economically while only using electric propulsion. The name "Blitzen" was chosen as it translates to flash or lightning in German while also being the name of a flight-capable high-speed guiding reindeer in Santa Claus stories. The team selected this name as the rotorcraft is designed to be a completely electric-powered flying form of rapid transport for passengers. Throughout the design process, the team consulted with distinguished industry leaders, experienced helicopter pilots, and eVTOL researchers. Using their valuable input, the Blitzen is spearheading the urban eVTOL air taxi market and will be able to generate significant revenue for operators.

Some of the most notable capabilities of the Blitzen are its ability to maintain a high lift to drag equivalent ratio of 7.4 at a cruise speed of 67.056 m/s (130.35 kts), redundant safety features, and low acoustic signature. By offloading lift from the main rotor to a wing and converting the tail rotor to a pusher propeller, the Blitzen can eliminate the necessity for main rotor shaft tilt, improving lift to drag ratio and decreasing noise. The vehicle is powered by ten electric motors providing a total of 1129 HP (842 kW) including excess power necessary in case of single motor failure, of which six are used for the main rotor and four for the swiveling rotorprop. For the comfort of all passengers, the Blitzen has 5.193 cubic meters (183.4 cubic ft) of cabin space and 1.634 cubic meters (57.7 cubic ft) available within the baggage compartment. In addition, the vehicle is designed to safely land at the closest suitable landing site (mission origin, alternate landing site, or mission destination) in the event of a single electrical component failure.

The Blitzen is an unconventional rotorcraft, combining traits of versatile compound helicopters such as the Airbus X^3 and Lockheed Cheyenne with transport helicopters such as the Bell 407 and the experimental Sikorsky S-61 RotoProp. The vehicles detailed dimensioned view is shown on the following page.

A. RFP Analysis

The RFP issued by Bell Helicopters includes the following recurring themes: safety during all mission components, ability to transport passengers with various types of disabilities, and use of electric propulsion. The RFP did not state many restrictions on vehicle design, allowing the team significant freedom in developing the configuration, propulsion, cabin, and rotor systems. The main restrictions are outlined in Table 1.

1. Safety and use of Electric Propulsion

The vehicle's sole power source is the array of onboard batteries. The RFP stipulates the use of idealized batteries that generate no heat and can provide full power until depleted. Due to the potential for single points of failure with electric battery systems, the vehicle must be able to continue safe flight following any single failure of the electrical system. Redundancy must be built in at every step to ensure the safe continuation of the mission. This can be returning to the departure site, diverting to an alternate landing zone, or continuing to the final destination location. Additionally, portions of 14 CFR 29 that pertain to small transport rotorcraft need to be complied with to ensure the safety of the crew, passengers, the vehicle, and other personnel on the ground.

2. Transportation of Passengers with Various Types of Disabilities

The RFP states that the vehicle must be able to transport at least two passengers with disabilities. This includes the passengers, their luggage, and necessary medical support equipment. Although some passengers may have visually identified disabilities, some can possibly have hidden or undetectable disabilities. The RFP indicates that careful consideration of the wider societal challenges faced by people with visible and hidden disabilities is encouraged and that the vehicle design should alleviate some challenges and barriers to transportation for as many people as possible.

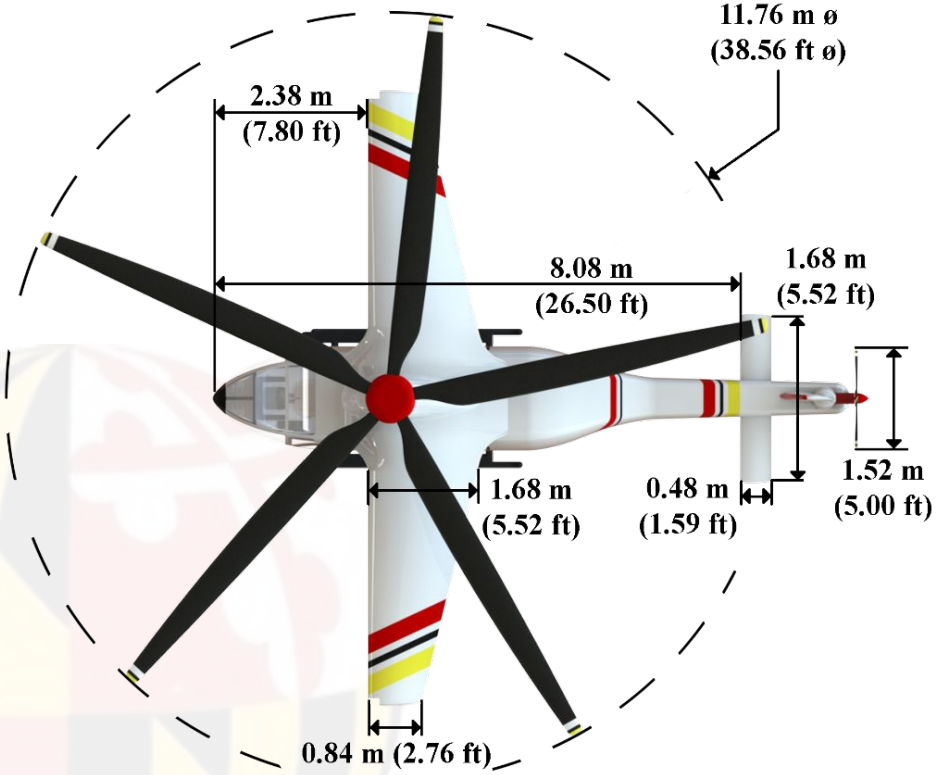

Footprint: 11.76 x 13.30 m
(38.56 x 43.65 ft)

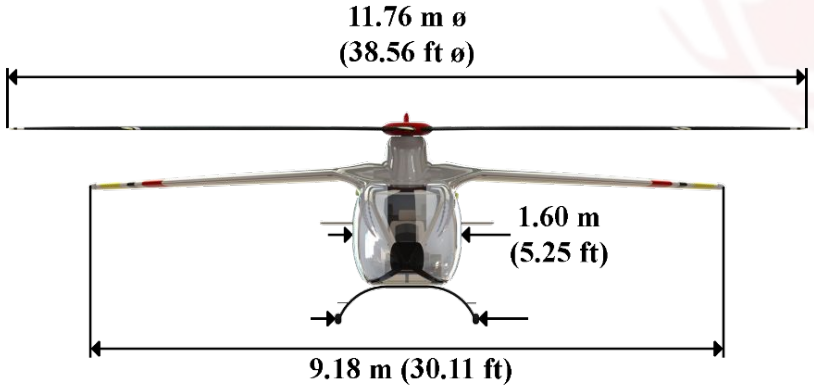

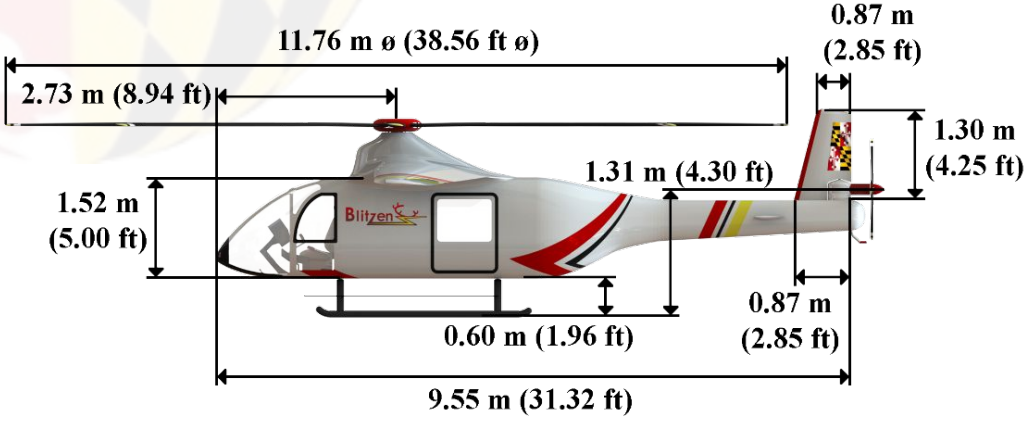

Table 1 RFP Compliance

RFP Requirements	Solutions	Chapter
Vehicle must be powered solely using batteries for electric propulsion. It must be able to fly 160.9 km (100 mi) without recharging.	Vehicle uses a distributed redundant electrical propulsion system running on six battery packs to achieve the desired range.	VIII, VII
The vehicle must be able to fly under single pilot operation and transport two people with disabilities or four fully mobile people in addition to luggage and medical support equipment.	The vehicle is designed to be flown by a single pilot and has a reconfigurable cabin capable of seating two or four passengers. A spacious cabin and luggage compartment accommodates all luggage and medical support equipment. Additional support equipment and operations are used for safe ingress, flight, and egress for all passengers.	XII, XIII
The vehicle must safely continue flight and land at either the departure location, alternate site, or destination in the event of a single electrical failure.	The vehicle has redundant electrical systems for motors, power distribution, batteries, and hover-to-cruise actuation.	VIII, VII, X
The vehicle must fit in 15.24 m (50 ft) by 15.24 m (50 ft) footprint.	The vehicle is sized to fit in a 15.24 m (50 ft) by 15.24 m (50 ft) footprint.	III
The batteries used onboard the vehicle are idealized with an energy density of 400 W-hr/kg (0.243 hp-hr/lb).	The battery system is sized with an energy density of 400 W-hr/kg (0.243 hp-hr/lb).	III, VIII
Rotor tip speeds cannot exceed 182.88 m/s (600 ft/s). Rotor blade twist must be linear.	Blitzen is sized to use a rotor tip speed of 152.4 m/s (500 ft/s) and linearly tapered rotor blades.	III, IV
System must be energy efficient.	The Blitzen employs a wing and pusher propeller in cruise to reduce power required and maximally increase overall energy efficiency.	IV, V
Overall Operational Safety	Blitzen prioritizes safety in every aspect of the design. This includes the pilot, passengers, vehicle, ground crew, and bystanders.	All

3. Mission Profile

The RFP includes a specific mission profile composed of eleven segments, and implies a need for cruise efficiency with a majority of flight time spent in the cruise phase. The prescribed mission (Figure 1) is that of a one-way rapid transport air taxi in an urban environment. The details of the individual flight legs are in Table 2. During this mission, the vehicle must transport two passengers with disabilities or four fully mobile passengers, including their luggage and equipment, from the departure location to the destination.

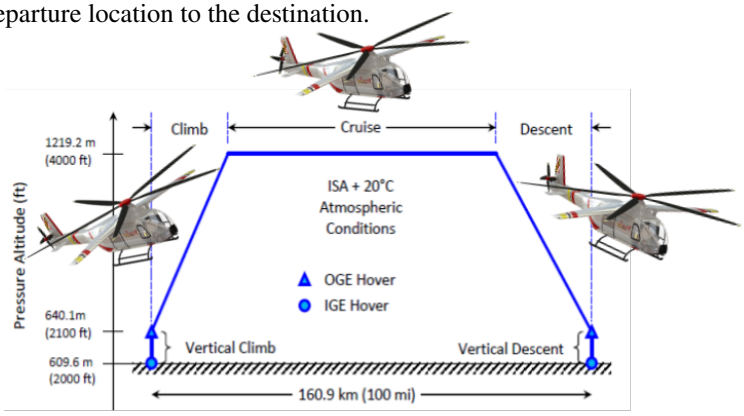

Fig. 1 Urban Air Taxi Mission Profile

Table 2 Mission Profile

Action	Description
Normal Vertical Takeoff to IGE Hover	The rotorcraft begins on the ground at 609.6 m (2000 ft) MSL at ISA+20C conditions.
In Ground Effect (IGE) Hover	After taking off, the rotorcraft will hover in ground effect for 10 seconds.
Vertical climb	The vehicle will climb vertically to 30.48m (100 ft) above ground level (AGL) at a rate of 48.77 m/min (160 ft/min).
Out of Ground Effect (OGE) hover	Once the rotorcraft reaches the vertical climb altitude, it will hover OGE for 10 seconds.
Inclined Climb	The helicopter will climb at an incline from its intermediate altitude to the cruise altitude of 1219 m (4000 ft) MSL at a 1:6 climb gradient. The team selected a 25 m/s (48.6 kts) forward flight speed for a 4 m/s (1000 ft/min) ascent rate.
Cruise	After reaching 1219 m (4000 ft) MSL, the rotorcraft will cruise for 149.2 km (92.7 mi). The team selected 67.06 m/s (130.35 kts) for Blitzen's cruise speed.
Inclined Descent	The inclined descent will decrease the rotorcraft's altitude to 640 m (2100 ft) MSL at a four degree angle. The team selected a 44.7 m/s (89.9 kts) forward flight speed for a 2 m/s (616 ft/min) descent rate.
OGE hover	Once the rotorcraft reaches the inclined descent altitude, it will hover OGE for 10 seconds.
Vertical Descent	The vehicle will descend vertically to 30.48m (100 ft) AGL.
IGE Hover	The rotorcraft will hover above the touchdown zone for 10 seconds in ground effect.
Normal vertical landing from IGE hover	The rotorcraft will safely execute a vertical landing from IGE hover.

II. Configuration Selection

The Blitzen is a single main rotor lift and thrust compounded aircraft designed for safety, cruise efficiency, ultra-low noise signature, and use of electric propulsion. Although the RFP provides scope for creativity, careful attention was given to the voice of the customer. A rigorous configuration selection process was conducted to identify three configurations to be analyzed in-depth, which is outlined in Chapter III. Analysis of the RFP, detailed in Section I.A, translated the voice of the customer to quantifiable metrics that can be compared to one another. This is transformed into design drivers derived from RFP information. Each driver is weighed against another in pairs to determine the ordered normalized priority vector using the Analytical Hierarchy Process (AHP). After ranking the drivers, a Pugh Matrix was developed using the normalized priority vector's scaling factors to rate each vehicle configuration quantitatively. Using this matrix, the three highest-ranking configurations were investigated in detailed trade studies.

A. Analytical Hierarchy Process (AHP)

The AHP process was used because it allowed for the exploration and consideration of a wide range of vehicle configurations to be narrowed down using the voice of the customer. The team was able to analyze the RFP and determine the characteristics of an ideal configuration for the customer. To accomplish this task, the team performed a comprehensive literature review using past University of Maryland designs, the VFS helicopter directory, the VFS eVTOL directory, and historical designs.

An AHP analysis was conducted to quantify the weights of design drivers derived from the RFP such that the Pugh Matrix for configuration selection can be scaled by the needs of the customer. The method involved the definition of the following design drivers.

1. Design Driver Formulation

Since the design drivers were created using verbiage directly from the RFP, each team member was assigned to subjectively interpret the needs of the customer. Individual interpretations were shared with the entire team to spark discussion of differing viewpoints. Throughout the process, each team member included their own perspective in the discussion to ensure that all desires of the customer were captured without missing nuances from individual RFP

evaluations. This yielded fifteen distinct parameters that were condensed to create eight design drivers. The final design drivers listed from higher to lower importance were:

1) **Passenger and Crew Safety** - The design must allow for safe ingress and egress of the pilot and passengers, including disabled passengers. Ensure safe continuation or termination of flight through operational redundancy or failsafe systems, including the safety of members on board the aircraft and personnel on the ground.
2) **Cater to All Disabilities** - An important aspect of the vehicle is its ability to transport a broad spectrum of travelers, including persons with reduced mobility (PRM). Disabilities can be easily visible or non-visible. All people should be able to access the services provided by the rotorcraft, regardless of their disability status.
3) **Minimization of Gross Takeoff Weight** - Minimizing Gross Take-Off Weight (GTOW) is tied to the performance of the powertrain, structure, and rotor. An increase in operational efficiency directly correlates to a reduction in aircraft weight.
4) **Range, Endurance, and Minimization of Block Time** - The RFP states that the rotorcraft has to have an operational range of 160.9 km (100 miles) with an additional 20 minutes of reserve cruise flight time available. Additionally, an air taxi is expected to transport passengers faster than ground-based taxis.
5) **Energy Efficiency (Battery and Engine)** - The battery has an energy density of 400 W-hr/kg (0.243 hp-hr/lb). Non-ideal, real-world effects such as battery lifetime and reduced available power at a low battery charge state can be neglected. The vehicle should maximize lift to drag ratio in cruise to decrease total energy usage. Efficiency of the electric motor and power system should be maximized to minimize the amount of battery energy required.
6) **Minimization of Vehicle Noise** - Due to the urban operation profile given by the RFP, noise inside and outside of the cabin should be minimized to reduce disturbances to the passengers and surrounding environment. Vehicle acoustics become a governing factor for suitable operating locations.
7) **Vehicle Initial and Operational Cost** - Vehicle cost determines clientele willing to use the taxi service. The total cost for design, testing, manufacturing, and operation will determine the constraints for the economic operation of the vehicle. Cost minimization encourages vehicle use in its intended air taxi role by the public, where price is not a limiting factor for widespread use.
8) **Mechanical Simplicity** - Mechanical simplicity promotes the design of components with minimal part counts. By reducing the number of parts, especially those that move or actuate, mechanical reliability increases. Maintenance also becomes much easier, timely, and affordable.

2. Analytical Hierarchy Matrix

After the design drivers were defined in detail and approved by all team members, the analytical hierarchy matrix, shown in Figure 2 was developed to rank the drivers into a normalized priority vector. The process included a full-team discussion to rate each design driver against one another to determine their relative importance.

Attribute:	Safety	Min. GTOW	Min. Vehicle Noise	Cost	Mechanical Simplicity	All Disabilities	Range/Endurance/Time	Energy Efficiency
Passenger and Crew Safety	0.3700	0.4149	0.2465	0.2666	0.2379	0.2998	0.2983	0.2927
Minimization of GTOW	0.0815	0.0847	0.1661	0.1103	0.1471	0.1466	0.1383	0.1726
Minimization of Noise	0.0737	0.0364	0.0418	0.1204	0.1018	0.0896	0.1238	0.0746
Vehicle Initial and Operational Cost	0.0712	0.0682	0.0641	0.0444	0.0951	0.0842	0.0565	0.0548
Mechanical Simplicity	0.0688	0.0485	0.0582	0.0678	0.0390	0.0520	0.0573	0.0437
Cater to All Disabilities	0.1505	0.1978	0.1711	0.1614	0.1547	0.0833	0.1943	0.1578
Range, Endurance, and Minimization of Block Time	0.1016	0.0702	0.1235	0.1061	0.1141	0.1265	0.0702	0.1468
Energy Efficiency - Battery and Engine	0.0828	0.0793	0.1288	0.1229	0.1102	0.1181	0.0612	0.0568
SUM	1.0000	1.0000	1.0000	1.0000	1.0000	1.0000	1.0000	1.0000

Fig. 2 Analytical Hierarchy Matrix

The column normalized analytical hierarchy matrix in Figure 2 generated the normalized priority vector in Table 3 by dividing each table element by its row sum. The result is a single vector that ranks each driver by their relative score. These values were used as weights for the configuration selection Pugh Matrix described in the next section.

Table 3 Normalized Priority Vector

Design Driver	Weight
Passenger and Crew Safety	30.33%
Cater to All Disabilities	15.89%
Minimization of Gross Takeoff Weight	13.09%
Range, Endurance, and Minimization of Block Time	10.74%
Energy Efficiency (Battery and Engine)	9.50%
Minimization of Vehicle Noise	8.28%
Vehicle Initial and Operational Cost	6.73%
Mechanical Simplicity	5.44%
Total	100%

To inspect the normalized priority vector in greater detail, we highlight a few design drivers that are most influential in our configuration selection. The most important driver for the design is **passenger and crew safety**; since this vehicle will be transporting passengers many times a day, ensuring the safety of the occupants in addition to the people and property external to the vehicle is paramount. Our second most important design driver is to **cater to all disabilities**. It is important to ensure that the potential clientele for this air vehicle includes passengers with visible and non-visible disabilities in order to provide high-speed taxi service to the entire public rather than for a select group of people. Designing a vehicle with such passengers in mind from the start ensures that most people will be able to conveniently use the air vehicle. Although passenger accommodations and comfort is required, **minimization of GTOW** is also important. Power required for hover and battery weight scales exponentially as GTOW increases, thus keeping GTOW low ensures efficiency in flight. In addition to minimizing weight, the vehicle must perform the required flight mission including **range and endurance** standards while **minimizing total block time for** passenger transport. People will likely use the air taxi as a significantly faster alternative to ground-based taxi services and individual ground vehicles. Lower scoring design drivers were not omitted in the design process and were factors that were considered in local analysis of each component within the rotorcraft detailed later in this proposal.

B. Configuration Selection using a Pugh Decision Matrix

In order to select the best vehicle configuration for the customer's mission, a study of major VTOL capable vehicle designs was performed. Using a Pugh matrix, the team ranked a wide variety of configurations with respect to the predetermined design drivers. The Single Main Rotor with Tail Rotor (SMR) helicopter configuration was used as a baseline comparison between all vehicles due to its widespread use. For this configuration, each design driver was rated a score of zero; this ensured that the vehicle's final score could be viewed as a control group. Each other configuration was rated an integer value between -3 (exceptionally poor) to +3 (exceptionally good), against the SMR for each design driver in order to rate the design's relative merit. The final scoring was determined by weighting the Pugh matrix solutions with the normalized priority vector, such that each design driver's relative importance scaled the final results.

	Weight	SMR Helicopter	SMR with Wing	SMR w/ Wing & Pusher	SMR Tiltwing /w pusher	SMR Lift Offset	Tandem Helicopter	Tandem with Wing	Multicopter Tiltrotor w/ wing	Multicopter Tilt Wing	Multicopter Ducted Tiltrotor w/ wing	Multicopter Stopped Rotor w/ pusher prop	Coaxial Helicopter	Coax w/ wing	Coax w/ wing and pusher	Multicopter	Stopped Rotor + Tiltrotor with Wing
Passenger and Crew Safety	0.3033	0.000	0.000	0.000	0.000	0.000	-0.303	0.000	0.303	-0.910	0.303	0.303	0.000	0.000	0.000	0.303	0.303
Minimization of GTOW	0.1309	0.000	-0.131	-0.131	-0.131	-0.131	-0.262	-0.131	-0.262	-0.262	-0.393	-0.262	-0.131	-0.262	-0.262	-0.131	-0.393
Minimization of Vehicle Noise	0.0828	0.000	0.083	0.166	0.166	0.166	-0.166	-0.083	0.166	0.166	0.248	0.166	-0.083	0.083	0.166	0.000	0.166
Vehicle Initial and Operational Cost	0.0673	0.000	-0.067	-0.067	-0.067	-0.067	-0.067	-0.135	-0.135	-0.202	-0.135	-0.067	-0.067	-0.135	-0.135	-0.067	-0.135
Mechanical Simplicity	0.0544	0.000	-0.054	-0.109	-0.163	-0.109	0.000	-0.054	-0.109	-0.163	-0.163	-0.109	-0.109	-0.109	-0.109	-0.109	-0.163
Cater to All Disabilities	0.1589	0.000	0.159	0.159	0.159	0.318	0.477	0.477	0.000	0.000	0.000	0.000	0.159	0.318	0.318	-0.159	0.159
Range, Endurance, Block Time	0.1074	0.000	0.107	0.215	0.107	0.107	0.000	0.107	0.215	0.215	0.215	0.107	0.000	0.107	0.107	0.000	0.215
Energy Efficiency (Battery and Engine)	0.0950	0.000	0.095	0.095	0.190	0.000	0.000	0.095	0.190	0.190	0.190	0.095	-0.095	0.000	0.095	-0.095	0.095
Sum	1.000	**0.000**	**0.191**	**0.327**	**0.260**	**0.284**	**-0.321**	**0.276**	**0.368**	**-0.967**	**0.266**	**0.233**	**-0.326**	**0.003**	**0.180**	**-0.258**	**0.247**

Fig. 3 Vehicle Configuration Pugh Matrix

The Pugh matrix shown in Figure 3 indicates that there are two configurations that strongly fit the requirements outlined by the customer. These configurations are the thrust and lift compounded SMR and the multicopter tiltrotor with wings. These two configurations, in addition to the conventional single main rotor helicopter, were selected for further detailed evaluation. A vehicle selection trade space was developed to compare these configurations intensively, which is documented in Chapter III. Flight-proven examples of each of these configurations are illustrated in Figure 4.

(a) Joby S4

(b) Bell 407

(c) Lockheed AH-56 Cheyenne

Fig. 4 Possible Vehicle Configurations Answering the RFP

1. Multicopter Tiltrotor with Wings

The multicopter tiltrotor is a VTOL capable vehicle using prop-rotors capable of 90 degree propulsive thrust vectoring. The same thrust elements used for vertical thrust hover are rotated to be used for forward propulsive force in forward flight. Tiltrotor eVTOLs designed specifically for urban air mobility, such as the Joby S4 (Figure 4a), are being tested currently. This vehicle design provides the hover capability of a conventional helicopter in addition to the forward flight aerodynamic efficiency of a fixed-wing aircraft. The tiltrotor promotes safety in two primary manners: redundant prop-rotors in a symmetrical layout about the vehicle's longitudinal-vertical plane and a wing capable of gliding. In the event of a single motor failure, a motor on the opposite side of the vehicle's plane of symmetry can be turned off or deliver power by cross-shafting for stable, but less efficient, flight. The tiltrotor has a high lift to drag ratio compared to a standard helicopter in cruise, complementing the long cruise segments prescribed in the RFP's mission profile. To hover and cruise with the same rotorprop, the configuration must compromise its blade geometry and structure for a high-velocity freestream axial flow in forward flight and static freestream conditions in hover. Additionally, the increased mechanical complexity of tilting mechanisms for each prop-rotor assembly raises component weight, vehicle cost, and maintenance cost. Finally, the configuration tends to have high disk loading. This may inhibit autorotative ability and can make the vehicle's downwash potentially dangerous to people or equipment near takeoff or landing zones.

2. Conventional SMR with Tail Rotor (SMR)

The single main rotor with tail rotor configuration is the most widely used and proven helicopter design. The configuration is currently used for VTOL transportation and can be considered as the main ultra-premium air taxi method today. The Bell 407 (Figure 4b) is a proven vehicle of this design style with over 1400 vehicles built. This configuration promotes redundancy as multiple motors can power the main rotor to continue safe operation in the event of a single motor failure. In addition, minimal moving parts in a mechanically simple rotor hub increases mechanism reliability. This design typically encompasses an increased autorotative capability by implementing a low disk loading. The lack of a wing simplifies ingress and egress procedures for passengers with disabilities. This configuration's widespread use is complemented by the vast network of trained pilots, mechanics, and operators who will not need retraining. Although some aspects of this configuration agree with the RFP, the lack of cruise efficiency limits its use solely under battery power. The effective lift to drag ratio of SMR vehicles tend to be lower than configurations with additional lifting or thrusting devices optimized for cruise. The cruise segment dominates the RFP's mission profile, thus a significantly higher battery weight is expected for this design over other considered configurations.

3. SMR with Thrust and Lift Compounding

The SMR configuration with thrust and lift compounding combines lift efficiency of a fixed wing aircraft in cruise and propulsive efficiency of a pusher propeller at high advance ratios resulting in fast forward flight and high cruise efficiencies. This configuration has been used in the past for vehicles such as the Lockheed AH-56 Cheyenne (Figure 4c) and Airbus X^3. This configuration's use of fixed-wing components allows lift offloading from the main rotor to the wing, causing it to exhibit a higher lift to drag ratio than a standard SMR in cruise. The vehicle's efficient propulsive thrust compounding removes the main rotor's need to tilt forward to counter parasitic drag in forward flight, further improving cruise efficiency. Similar to the conventional SMR, this configuration promotes operational redundancy with multiple motors driving a single rotor shaft. Full operation is possible in a one motor inoperative (OMI) scenario. The low disk loading of the main rotor allows exceptional autorotative capability given a total electrical failure. This configuration's increased efficiency in cruise flight comes at a cost to more power required in hover from main rotor wake impingement by the wing. Additionally, the wing must be strategically placed to avoid interfere with the ingress and egress procedure for a disabled passenger.

III. Vehicle Trade Studies and Sizing

In order to select a final vehicle configuration from the three listed in Section II.B, a detailed trade study was performed to quantitatively compare each vehicle's parameters and their agreement with the requirements in the RFP. This included vehicle sizing investigations using momentum theory and rotor and propeller configuration studies using blade element momentum theory. The trade space results summary used to compare each configuration is in Table 4. This table was informed by analysis described further in this section.

Table 4 Trade Space Summary

Parameter	Multicopter Tiltrotor	SMR	SMR Compound
Vehicle GTOW	2610.9 kg (5756 lb)	2575.5 kg (5678 lb)	2648.5 kg (5839 lb)
Cruise Speed	67.06 m/s (130.35 kts)	53.6 m/s (104.28 kts)	67.06 m/s (130.35 kts)
Cruise Total Equivalent Drag Area	0.662 m^2 (7.13 ft^2)	0.656 m^2 (7.06 ft^2)	0.669 m^2 (7.2 ft^2)
Mission Completion Time	45.96 min	52.97 min	45.96 min
Number of Rotors	6 (Hexagon Spacing, Tilting)	1 Main + tail	1 Main + tail/pusher
Rotor Radius	1.64 m (5.39 ft)	6.04 m (19.81 ft)	5.87 m (19.28 ft)
Rotor Solidity	0.1592	0.0749	0.0936
Rotor Blade Twist (Root-to-tip)	-7°	-12°	-9°
Rotor Blade Bi-taper (Transition=0.6R)	1.5 & 1	2 & 1	2 & 1
Rotor Tip Speed	167.6 m/s (550 ft/s)	152.4 m/s (500 ft/s)	152.4 m/s (500 ft/s)
Special Features	Wing and Tilting Pods	-	Wing, Swiveling Tail Rotor
OGE Hover Figure of Merit (FM)	0.83	0.83	0.84
IGE Hover Single System Failure FM	0.70	0.80	0.80
Hover Power Required	622.5 kW (834.8 hp)	382.3 kW (512.7 hp)	517.1 kW (703.2 hp)
Vertical Climb Power Required	691.43 kW (927.22 hp)	418.3 kW (561.3 hp)	556.34 kW (746.07 hp)
Angled Climb Power Required	25.4 kW (34.1 hp)	339.4 kW (455.1 hp)	100.66 kW (134.99 hp)
Cruise Power Required	156 kW (209.3 hp)	258.1 kW (346.1 hp)	236.05 kW (316.54 hp)
Angled Descent Power Required	26.7 kW (35.9 hp)	119.9 kW (160.8 hp)	69.14 kW (92.71 hp)
Vertical Descent Power Required	503.8 kW (675.6 hp)	372.0 kW (498.9 hp)	395.5 kW (530.38 hp)
Total Installed Power	1247 kW (1672 hp)	484 kW (649 hp)	607 kW (814 hp)
Hover Energy Consumed	1.73 kW-Hr (2.32 hp-Hr)	1.06 kW-Hr (1.42 hp-Hr)	1.45 kW-Hr (1.94 hp-Hr)
Vertical Climb Energy Consumed	5.69 kW-Hr (7.64 hp-Hr)	4.36 kW-Hr (5.85 hp-Hr)	4.62 kW-Hr (6.19 hp-Hr)
Angled Climb Energy Consumed	1.02 kW-Hr (1.37 hp-Hr)	10.75 kW-Hr (14.41 hp-Hr)	4.05 kW-Hr (5.43 hp-Hr)
Cruise Energy Consumed	96.4 kW-Hr (129.28 hp-Hr)	199.34 kW-Hr (267.32 hp-Hr)	145.84 kW-Hr (195.57 hp-Hr)
Angled Descent Energy Consumed	2.15 kW-Hr (2.89 hp-Hr)	6.17 kW-Hr (8.29 hp-Hr)	5.56 kW-Hr (7.46 hp-Hr)
Vertical Descent Energy Consumed	5.25 kW-Hr (7.04 hp-Hr)	3.87 kW-Hr (5.20 hp-Hr)	4.12 kW-Hr (5.52 hp-Hr)
Total Energy Consumed	117.4 kW-Hr (157.5 hp-Hr)	228.74 kW-Hr (306.74 hp-Hr)	169.97 kW-Hr (227.93 hp-Hr)
Reserve Energy	52.01 kW-Hr (69.8 hp-Hr)	86.04 kW-Hr (115.4 hp-Hr)	78.68 kW-Hr (105.51 hp-Hr)
Total Battery Weight	489.6 kg (1079 lb)	909.4 kg (2005 lb)	719.4 kg (1586 lb)
Propulsion Max. Continuous Torque	12,330.0 N-m (9094.1 ft-lb)	21,200.0 N-m (15,636.0 ft-lb)	24,750.0 N-m (18,254.7 ft-lb)
Propulsion Max. Continuous Power	1256.7 kW (1685.3 hp)	535.1 kW (717 hp)	642.0 kW (861 hp)
Tail Max. Continuous Torque	N.A.	375 N-m (276.6 ft-lb)	862.3 N-m (636.0 lb-ft)
Tail Max. Continuous Power	N.A.	87 kW (116.7 hp)	200 kW (268.2 hp)
Transmission Method	Geared	Geared	Geared

A. Sizing Methodology

An in-house sizing code was developed (see flowchart in Figure 5 using modified momentum theory to model helicopter aerodynamics in hover, climb, cruise, and descent [6, 7]. Initial conditions for the code included the

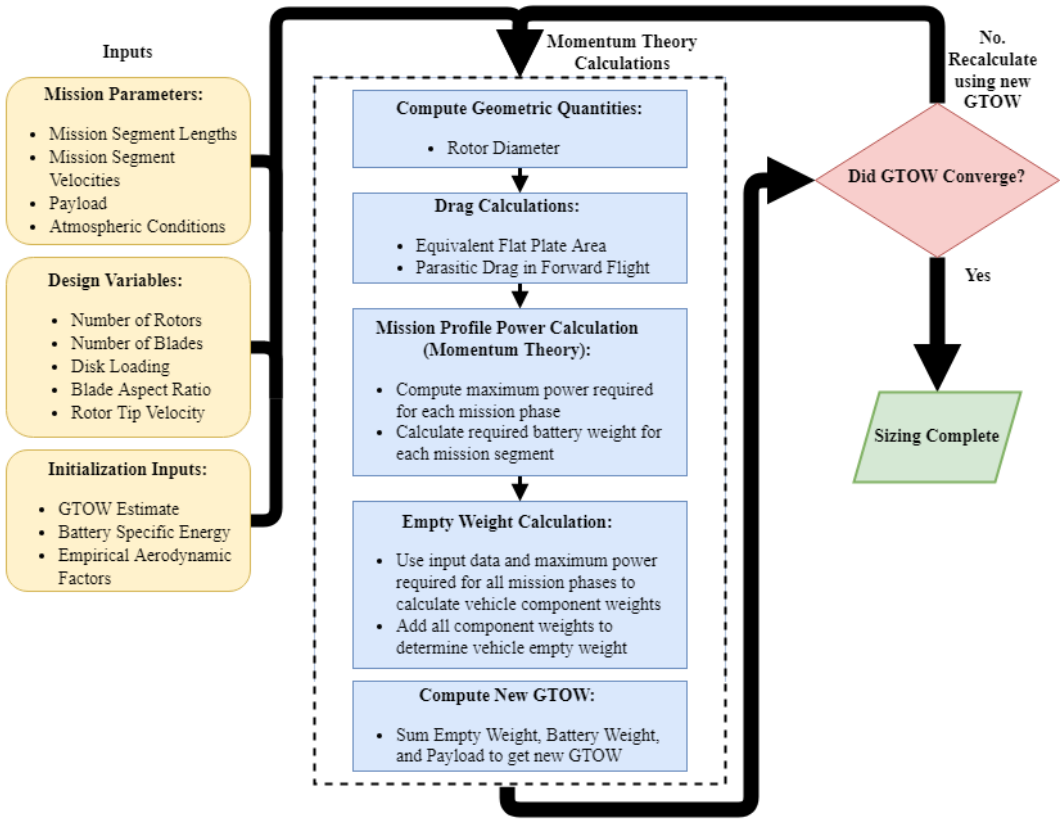

Fig. 5 Flowchart of Vehicle Sizing Code Procedure

idealized battery specific energy of 400 W-hr/kg (0.243 hp-hr/lb), estimated payload of 5337.9 N (1200 lb), and other constraints set by the RFP. Power required for each flight phase dictated required battery weight. Weights of conventional helicopter subcomponents were derived from initial conditions and maximum power required among all flight segments. Equations from Tischenko's methodology and Aero Flight Dynamics Directorate (AFDD) [7] developed using statistical approximations were used to calculate the component weights. eVTOL specific component weights were referenced from Kadhiresan and Duffy [8]. Motors were sized using continuous required power, as advised by Whiteside et al. [9]. Additional technology factors published by NASA's Dr. Wayne Johnson scaled equation outputs to realistic approximations for eVTOL component weights [10]. The vehicle empty weight, payload, and battery weight were used as a new GTOW inputs for the next code iteration. The code iterated until the GTOW converges within a fixed error tolerance to the previous iteration's GTOW. Pertinent vehicle parameters, such as power required for each rotor, GTOW, battery weight, rotor diameter, blade loading, advance ratio, and other notable values were outputs from the code after GTOW convergence.

1. Sizing Code Drag Estimation

Initial forward flight drag estimation within the sizing code computes parasitic drag force and power required to overcome this drag using equivalent flat plate area for vehicle fuselages and rotors. Parasitic drag is calculated using Equation (1) where q is dynamic pressure and f is equivalent flat plate area. The sizing code estimates equivalent area using Equation (2) from [11] where GTOW is in pounds and K is a scaling factor ranging from 2 to 2.9 for the best streamlined vehicles to non-optimized designs respectively.

$$D = qf \tag{1}$$

$$f = K\left(\frac{GTOW}{1000}\right)^{0.7263} \tag{2}$$

In addition to parasitic drag, wing induced and profile drags are calculated for the compound SMR and multicopter tiltrotor configurations. Wing loading, Oswald span efficiency factor, wing aspect ratio, and wing area are used to compute the two parameters. The wing drag is added to fuselage drag to compute propulsive power in forward flight.

2. Sizing Code Estimation of Hover Download due to Wake Impingement

Hover download due to rotor wake impingement was accounted for in the sizing code. A constant 2%, 15%, and 16% of GTOW was additionally applied to the SMR, multicopter tiltrotor, and compound SMR respectively to account for this download. These scaling factors were calibrated using reference vehicle parameters published by Duffy et al. for various vehicle configurations [12].

3. Sizing Code Miscellaneous Power Consumption and Energy Losses

Electrical power is primarily used for vehicle lift and propulsion. Equipment such as avionics, deicing, and flight controls consume additional power. An additional one percent and three percent of rotor power in cruise and hover respectively were allocated for miscellaneous power consumption.

Power losses from motor efficiencies and energy losses from imperfect batteries were factored into the sizing code. Vehicle installed power was increased from the required power to account for an 85% efficient motor. Battery energy was also increased over the calculated total mission energy assuming an 87% efficient battery is used.

B. Code Validation

The sizing code required validation against published data before conducting trade studies since it was developed in-house by the team. Initially, the hover and cruise scripts were configured with a specific fuel consumption for comparison with Robinson R-66 flight test data with blade loading of 0.102. The code validation is depicted in Figure 6. The plot indicates good correlation between the code and R-66 flight test data, with a maximum of 10% overprediction at mid to high advance ratios. The calculated data points from the code has thus been validated and accurate enough to convert to sizing vehicles using electric propulsion.

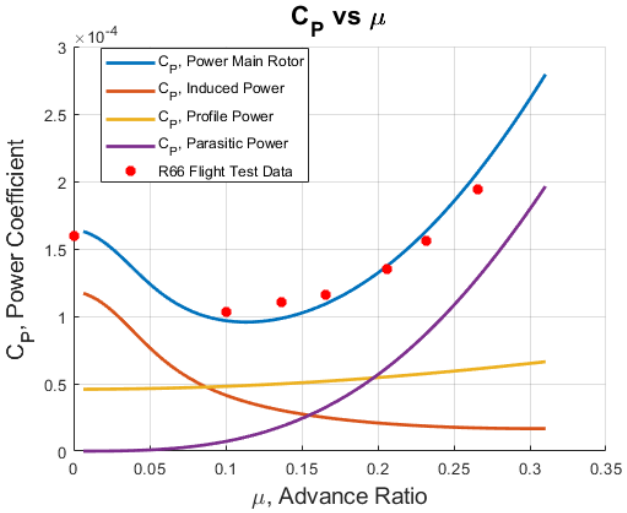

Fig. 6 Initial Sizing Code Validation with Flight Test Results of the R-66 Helicopter

After the hover and cruise scripts were validated for the turbine engine powered vehicle, the code was converted to sizing vehicles using electric propulsion systems. This code was further validated against Duffy et al.'s published vehicle parameters for an electric conventional SMR configuration and winged multicopter tiltrotor configuration [12]. All pertinent vehicle output parameters such as rotor diameter, hover/cruise/installed power, empty weight, GTOW, battery weight, power loading, etc. agreed with Duffy et al. within 6%. This deviation was deemed acceptable this early in the design process, allowing continuation of the configuration trade study.

C. Cruise Speed Selection

Vehicle sizing depended heavily on cruise speed because this, and thus cruise time, primarily determined the total mission's required energy. The team assigned minimization of block time as a high priority design driver. A typical ground taxi cruises at 26.8 m/s (52.14 kts), causing the full mission profile to take 100 minutes if travelling in a straight line. At 53.6 m/s (104.28 kts), the travel time is halved, to 50 minutes. At 67.06 m/s (130.35 kts), an additional 10% decrease in travel time is provided. High advance ratios and large increases in parasitic drag at high cruise velocities encouraged the team to select 67.06 m/s (130.35 kts, 150 mph) as the vehicle's maximum cruise speed.

D. Sizing Aerodynamic Parameters Trade Studies

A fair comparison between the three configurations examined in this trade space (multicopter tiltrotor, SMR, lift and thrust compounded SMR) requires the selection of vehicle parameters for each design to best align with the RFP. The sizing code is capable of performing a parametric sweep of various main rotor disk loadings (DL), number of blades, and rotor tip velocities. Carpet plots of these parameters against GTOW, installed power, and rotor diameter were used to determine the aerodynamic parameters of each configuration in the trade space. The SMR configuration's carpet plots featuring isolines for rotor tip velocity and blade count are illustrated in Figure 7. Similar plots were generated for the other configurations. All data points plotted feature blade loadings (C_T/σ) below 0.12 to ensure sufficient maneuvering margin before the onset of blade stall.

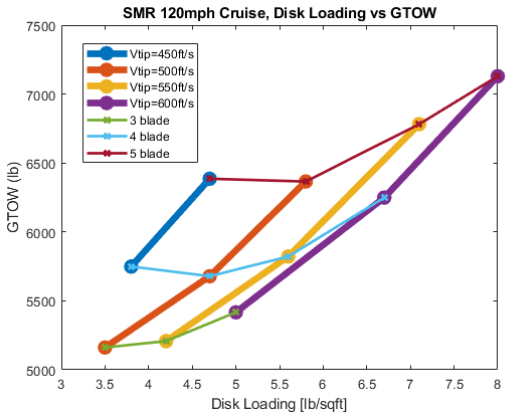

(a) SMR Trade Study 1: DL vs $GTOW$

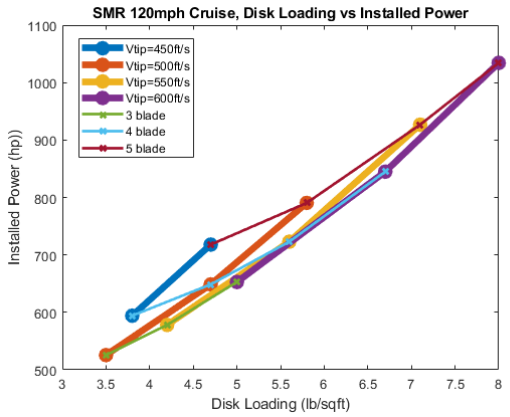

(b) SMR Trade Study 2: DL vs $P_{installed}$

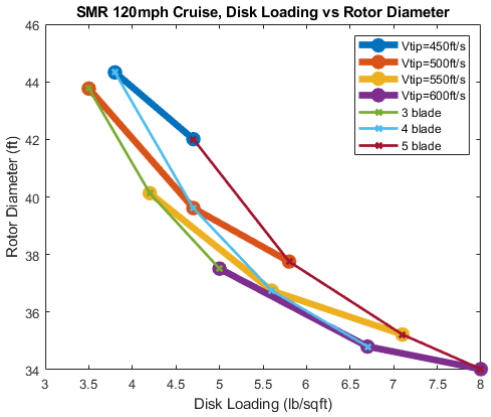

(c) SMR Trade Study 3: DL vs $RotorDiameter$

Fig. 7 Electric SMR Configuration Trade Study

Table 5 is a summary of vehicle parameters selected for the three configurations in the trade space obtained using the sizing code.

Table 5 Vehicle Parameters Obtained using the Sizing Code

Parameter	Multicopter Tiltrotor	SMR	SMR Compound
GTOW	2610.9 kg (5756 lb)	2575.5 kg (5678 lb)	2648.5 kg (5839 lb)
Installed Power	1247 kW (1672 hp)	484 kW (649 hp)	607 kW (814 hp)
Number of Rotors	6 (Hexagon Spacing, Tilting)	1 Main + tail	1 Main + tail/pusher
Disk Loading	67.06 m/s (150 mph)	53.6 m/s (120 mph)	67.06 m/s (150 mph)
Rotor Diameter	3.29 m (10.8 ft^2)	12.07 m (39.61 ft)	11.75 m (38.56 ft)
Blade Aspect Ratio	10	17	17
Number of Blades	5 per rotor	4	5
Rotor Tip Velocity	167.6 m/s (550 ft/s)	152.4 m/s (500 ft/s)	152.4 m/s (500 ft/s)
Special Features	Wing and Tilting Pods	-	Wing, Swiveling Tail Rotor

1. Configuration 1: Multicopter Tiltrotor

The multicopter tiltrotor's configuration (Figure 8) was selected to minimize power required in cruise while ensuring that the vehicle fit within the 15.24 m (50 ft) by 15.24 m (50 ft) footprint limit. Sizing was performed with the assumption of single motor failure requiring shutdown of the symmetric motor on the opposite side of the vehicle. Six

tilting rotor/propellers were selected as thrust elements such that the large 3.29 m (10.8 ft) diameter rotors attached to a wing could fit within the design footprint. A higher rotor count decreases total required power in the event of a single motor failure, however, geometric constraints limited the vehicle to six rotor pods in a tractor configuration which rotate upwards in hover. Additional rotor/propellers could be added as pushers and rotate downwards in hover, though they would block doors used for ingress and egress. A parametric sweep of rotor blade count, disk loading, and installed power was performed to select a single configuration with desired characteristics detailed in Table 5. The blade aspect ratio was fixed to allow solidity to vary solely by blade count, as $\sigma = \frac{N_b}{\pi AR}$. The study revealed a favorable configuration balancing low GTOW, decreased acoustic signature with a high blade count and reduced rotor/propeller tip velocity, and smaller rotor diameter.

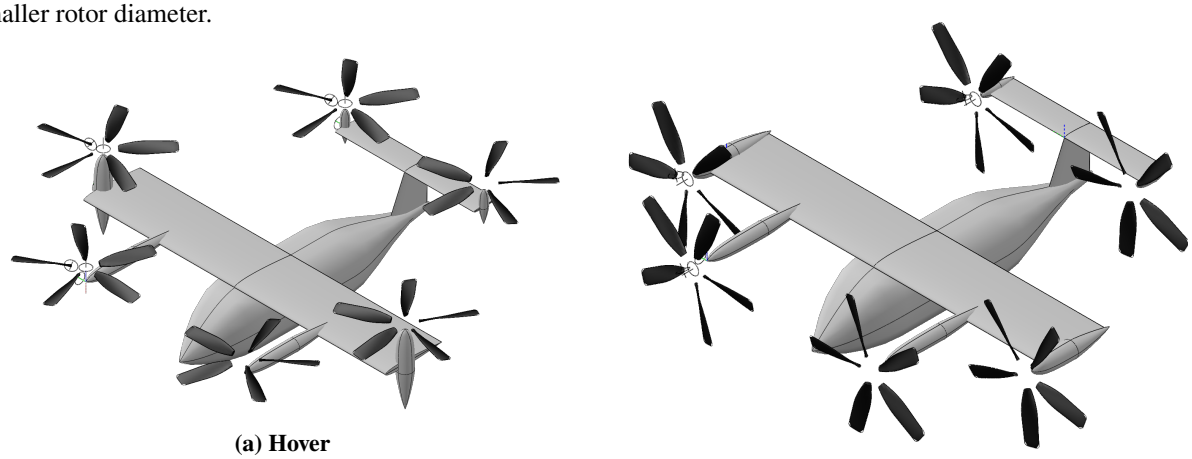

(a) Hover

(b) Cruise

Fig. 8 Tiltrotor Configuration with Chosen Vehicle Parameters

2. Configuration 2: SMR

The SMR configuration's (Figure 9) disk loading, blade count, and tip velocity were chosen to balance minimization of GTOW and installed power while allowing the vehicle to fit within the 15.24 m (50 ft) by 15.24 m (50 ft) footprint prescribed in the RFP. A 12.19 m (40 ft) rotor diameter was considered as an upper limit to ensure sufficient space for the tail rotor. The assumed main rotor to tail rotor diameter ratio of 5:1 allotted 0.61 m (2 ft) of buffer space between the main rotor and tail rotor. In order to develop a vehicle that fit within this footprint, the maximum cruise velocity was decreased to 53.6448 m/s (120 mph). The blade aspect ratio was fixed, to allow solidity to vary solely by blade count. The study revealed a vehicle with minimum GTOW, low rotor tip velocity, and a low installed power relative to other parametric configurations while maintaining a rotor diameter below 12.19 m (40 ft), shown in Table 5.

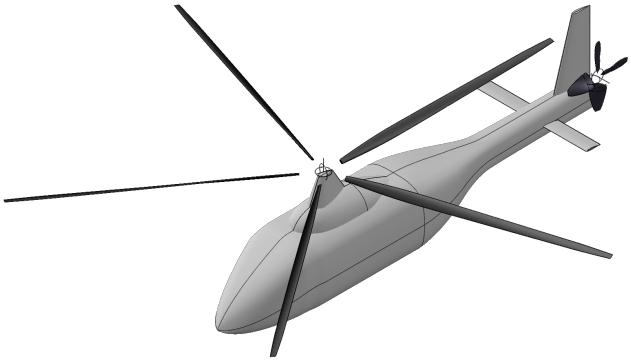

Fig. 9 Single Main Rotor and Tail Rotor Configuration with Chosen Vehicle Parameters

3. Configuration 3: Lift and Thrust Compounded SMR

The compound SMR's (Figure 10) aerodynamic parameters were determined in a similar manner to those of the conventional SMR, for example, a 12.19 m (40 ft) rotor diameter upper limit still applies to this configuration. The sizing code's climb, cruise, and descent segments were modified to offload up to 80% of required lift from the main rotor to the wing and transfer the main rotor's propulsive thrust requirements to the pusher propeller. This increased cruise L/D_e. However, additional empty weight was added to account for the wing and pusher propeller, increasing required power in hover. As displayed in Table 5, the study revealed a parameter configuration with low GTOW, rotor tip velocity, and installed power while ensuring a rotor diameter below 12.19 m (40 ft).

Historical compound helicopters, such as the Lockheed Cheyenne and Airbus X^3, include a pusher propeller in

addition to a tail rotor or a pair of propellers connected to the main gearbox. The electric powerplant required by the RFP presened a unique opportunity to have independent motors for the main rotor, tail rotor, and pusher propeller. A swiveling rotorprop can act as a tail rotor in hover and a pusher propeller in cruise while using the same motors in both configurations. A lightweight swivel actuation system and rudder control surface for yaw control in forward flight can be introduced. In cruise, yaw control is provided from the vertical stabilizer and rudder. These extra weights were offset by the removal of the tail drive shaft and duplicate tail rotor/pusher propeller. A thrust compound trade study was conducted to determine how installed power and GTOW varied between the standard thrust compounding empennage configuration and the swiveling rotorprop. Main rotor parameters remained constant. The results of this study are summarized in Table 6.

Table 6 Thrust Compound Empennage Trade Study

Configuration	Total Installed Power	GTOW
Separate TR and Pusher Prop	618.78 kW (829.8 Hp)	2718.6 kg (5993.5 lbs)
Swiveling Rotorprop	606.6 kW (813.5 Hp)	2648.3 kg (5838.6 lbs)

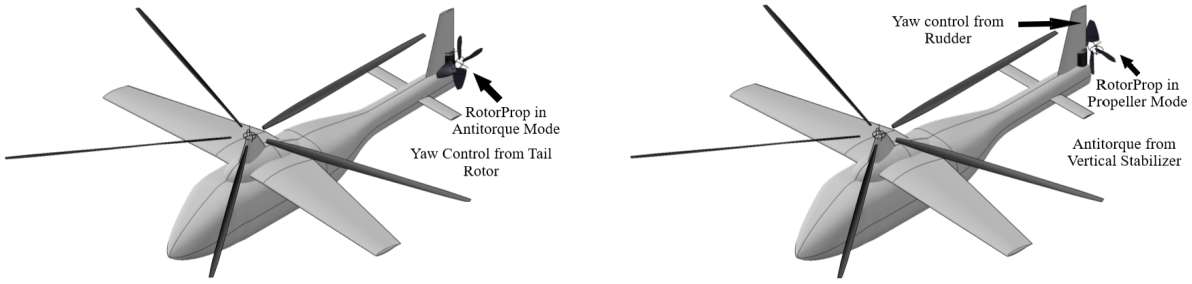

(a) Hover **(b) Cruise**

Fig. 10 Lift and Thrust Compounded SMR Configuration with Chosen Vehicle Parameters

4. Configuration Cruise Power and Energy Comparison

Although each vehicle in the trade space can complete the mission successfully, they each present high efficiencies in differing mission segments. A performance comparison was made between the three configurations with respect to their required power and cruise segment energy versus flight velocity (Figure 11). The SMR is most efficient in hover. The compound and tiltrotor configurations require 31.4% and 47.9% additional power in hover respectively. The lack of wake impingement-caused download, higher power loading, and low disk loading decreases required power for the SMR. At cruise velocity, the tiltrotor configuration requires the lowest power. The SMR and compound configurations require 83% and 38% additional power in cruise respectively. The tiltrotor benefits from applying all thrust elements to propulsive force and a high L/D_e from the wing.

The required energy plot conveys similar trends to the required power plot. The SMR requires the least energy to complete the mission at very low forward velocities due to its minimal total hover power. The tiltrotor needs the least power at high cruise velocities. The compound helicopter requires slightly more energy than the SMR at low velocities, needs the least energy at moderate-high velocities and slightly more energy than the tiltrotor at high velocities.

Since the SMR and tiltrotor are ultra-optimized for one end of the flight velocity spectrum, neither can perform both hover and cruise of the mission very well. The compound SMR configuration is a desirable compromise between the tiltrotor and SMR. It requires relatively low-moderate power in hover and cruise.

Table 7 Varied Geometries for Main Rotor Designs

Geometry Type	Values
Airfoils Varied	NACA0012
	Clark-Y
	OA212/OA209
	RC4-10/RC3-8
Inboard Taper	1:1 to 2.5:1
Outboard Taper	1:1 to 2:1
Taper Transition	0.4R to 0.6R
Single Linear Twist	-6°/span to -12°/span

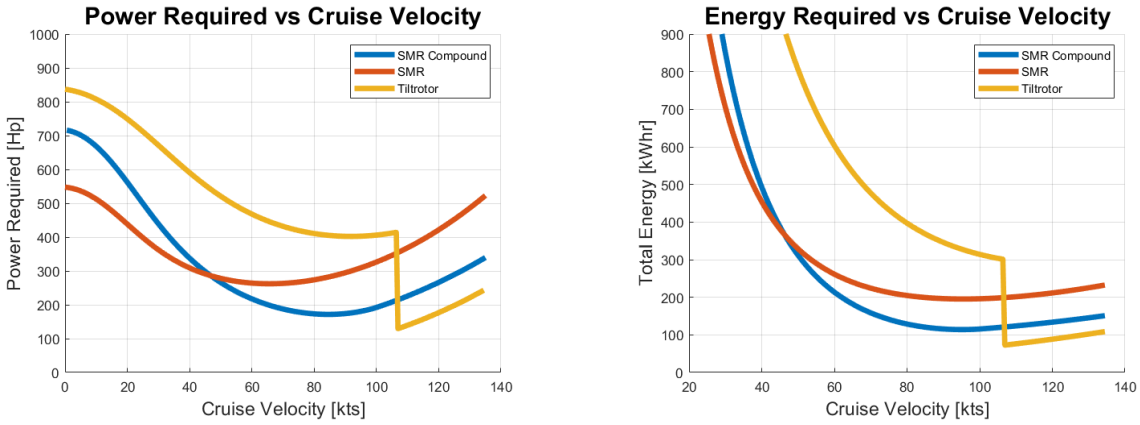

(a) Power Required vs Flight Velocity **(b) Cruise Energy Required vs Flight Velocity**

Fig. 11 Vehicle Performance Trade Study

E. Rotor Design Trade Studies

The sizing code computed power required for the rotors using a uniform inflow profile. The in-house Blade Element Momentum Theory (BEMT) code was developed by the team to understand aerodynamic characteristics along a rotor blade. Rotor blade geometries for each vehicle configuration were evaluated using this code.

Main rotor design for each configuration used one airfoil throughout blades for geometric simplicity and ease-of-fabrication. To generate main rotor designs for all three configurations, airfoils, taper ratio, twist, and their respective transition regions were considered for each rotor blade. The RC3-8, RC4-10, OA212, OA209, NACA0012 and Clark-Y airfoils were compared with the goal of achieving overall high performance results in hover and cruise. Table 7 provides the summary of all tested parameters.

Figure 12 presents two-dimensional aerodynamic coefficients C_l and C_d versus angle of attack α for a single Reynolds number (Re). Re of $2*10^6$ at n_{crit} = 9 was chosen since it is the average of the trade space. As required by the RFP, the blade twist angle was kept linear.

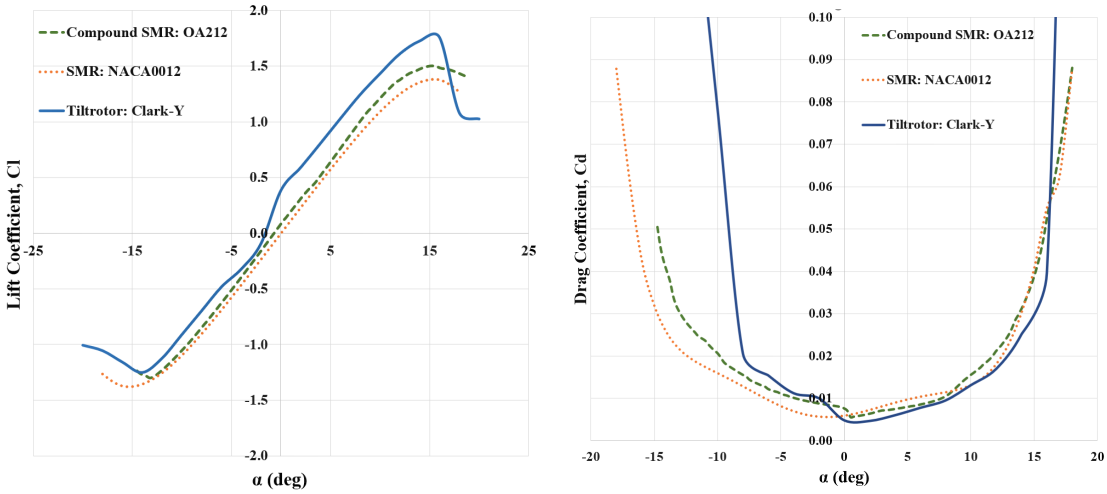

(a) C_l vs α **(b) C_d vs α**

Fig. 12 Aerodynamic Coefficients vs Angle of Attack at Re= $2*10^6$

All designs took advantage of a bilinear taper with the transition point at 60% of the blade radius. Due to uniform inflow distribution, the induced component of power is at its minimum when the rotor is in hover. Applying negative twist angle will reduce the usage of induced power. Particular twists and tapers that were computed for each configuration

are shown in Table 4. The OA212 airfoil was chosen for the compound helicopter configuration since it produces the highest FM in hover. The NACA0012 airfoil was selected for the SMR configuration since it is a symmetrical airfoil benefiting from a Lift-to-Drag ratio. Since the SMR configuration does not have a wing to offload lift from the MR in forward flight, having high L/D is beneficial compared to other tested airfoils. The multicopter tiltrotor is a vectored thrust configuration with 6 rotors. It is important to consider its dual function of a rotor in hover and a propeller in forward flight. Since this eVTOL spends most of its time in forward flight, the Clark-Y airfoil was chosen because it provides a high efficiency in propeller mode.

For each blade design, a 20 % root cutout was selected to provide sufficient space for the hub and mitigate weight and drag from unproductive blade sections in cruise. Additionally, each blade geometry Prandtl's tip loss factor into account as a result of the wake.

As required by the RFP, Figure 13 presents a plot of power coefficient vs. thrust coefficient in hover for all three configurations at the 75% blade radius position. The generated plots consider variation of twist angle and taper which serve as ones of primary parameters in characterizing the aerodynamic performance of the main rotor. Axial and tangential flows remain the same throughout the mission for each configuration as rotor tip velocity and cruise speed is constant.

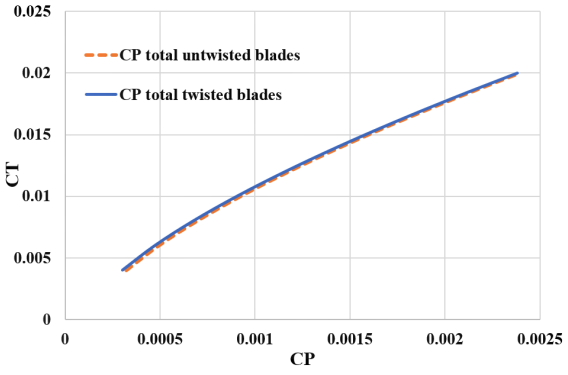

(a) SMR: C_T vs C_P

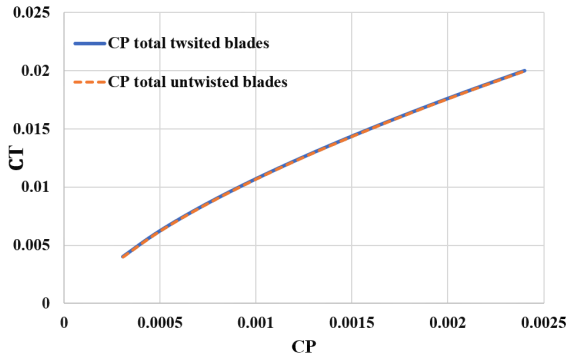

(b) Multicopter Tiltrotor: C_T vs C_P

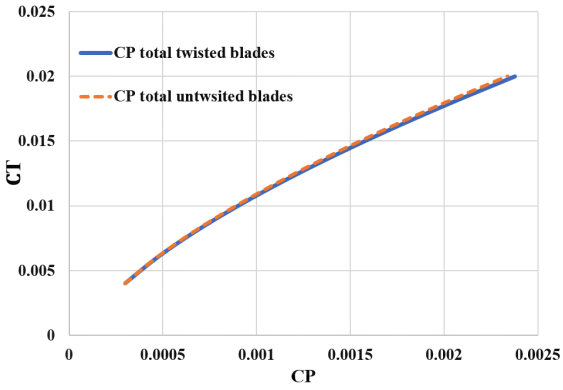

(c) Compound Helicopter: C_T vs C_P

Fig. 13 C_T vs C_P for Varied Twist of MR Blades in Hover

Each plot contains a curve for an untwisted and a twisted blade. As shown in Figure 13, little difference is visible between the twisted and untwisted blades for each rotor configuration. Since the range of C_T, which is consistent with the configurations' performance, is quite low, the effect of twisted blades specifically on rotor performance is not notable when plotting C_T against C_P. C_T and C_P are critical performance metrics that, when dimensionalized, can be used to characterize flight efficiency in hover and cruise. Every C_T vs C_P plot looks similar, as no rotor blades exhibit stalling during normal hover operations.

F. Lifting Surfaces Trade Study

Various combinations of lifting surfaces were used for the three vehicle configurations analyzed in the trade study. It is important to characterize and compare the control and stall characteristics of each lifting surface.

1. Wing Trade Study

The multicopter tiltrotor and compound helicopter configurations feature wings to improve cruise L/D_e. During hover, the wings of both configurations are stalled. Forward acceleration from the lifting rotors generates airflow over the wings during transition to cruise. Rotors continue to provide necessary thrust for the vehicle until the wings are completely non-stalled to mitigate transition stall effects.

Rotor wake download from the wing is higher for the compound SMR compared to the tiltrotor, as more wing area is covered by rotor disk area. However, the compound SMR does not need to include ailerons in the wing to control roll in cruise since the main rotor cyclic control is still active.

2. Horizontal and Vertical Stabilizer Trade Study

Horizontal and vertical stabilizers are present in all configurations. Both surfaces are stalled in hover flight for all three vehicles. The stabilizers are used to counteract adverse pitching and yawing moments induced by the fuselage and rotors respectively.

The horizontal stabilizer is required during cruise for every configuration, as fuselage induced pitching moments are highest in that flight phase. Similar to the wing, the horizontal stabilizer gains effectiveness as forward flight velocity increases. An elevator is required on the tiltrotor's horizontal stabilizer due to the loss of rotor pitch authority in cruise, therefore adding weight. For both configurations, rotors are able to provide pitch control when the horizontal stabilizers are stalled.

The vertical stabilizer is required in cruise for the compound SMR and tiltrotor configurations. Both must use a rudder because the rotor(s) lose yaw authority in forward flight. In addition, the SMR and SMR compound configurations use the vertical stabilizer to provide main rotor anti-torque. The SMR can decrease tail rotor power in cruise and the SMR compound can limit constant rudder deflection. For all configurations, the rotors are capable of providing yaw control or anti-torque when the vertical stabilizers are stalled.

G. Motor and Drive System Trade Studies

Among the three configurations, the multicopter tiltrotor requires the highest installed powers. Due to the single power system failure constraint and the high installed power requirement, it was very difficult to find a feasible motor to power it while keeping weight low. The SMR configuration requires less power for hover but needs the highest power for cruise. The increase of power required during cruise increases aircraft weight due to the need for more onboard energy storage. The compound SMR configuration requires slightly more power than the conventional SMR in hover but featres much lower required power in cruise. Because of this lower power requirement in cruise, the motors would require less power which would increase the efficiency of during the cruise portion of the mission, which is the longest portion of the mission.

The drive systems for each of the trade study configurations closely align with the motor selections. For the multicopter tiltrotor, having a tilting gearboxes for each of the six rotors will significantly add to the weight and complexity of the system. The SMR and SMR compound configurations would have similar drive systems for the main rotor, but the compound version has added mechanical complexity at the rear, because of the swiveling rotorprop.

H. Trade Study Summary

The trade space has been fully defined for the three configurations: Multicopter Tiltrotor, Single Main Rotor with Tail Rotor, and Single Main Rotor with Thrust and Lift Compounding. To select a final vehicle configuration, a side-by-side quantitative comparison (Table 4) of pertinent parameters was conducted. As this is a high speed urban electric air taxi, the balance of the following highly important parameters guided the final configuration selection: mission completion time, rotor blade count and tip speed for acoustics, maximum power required (highest segment power required + OMI), total energy consumed, battery weight, and GTOW. These parameters align with the design drivers generated early in the design process.

1. Final Configuration Selection

By comparing all parameters in the trade space, the **lift and thrust compounded SMR** configuration was selected. It features a full wing for main rotor lift offloading and propulsive thrust compounding using a swiveling tail rotorprop.

Over the other configurations, it has a relatively low cruise power requirement, a moderate hover power requirement, low rotor tip velocity and thus low acoustic signature, high available cabin volume, distributed redundant motors for the main rotor, and few components varying function in hover and cruise.

IV. Main Rotor and Wing Design

A. Main Rotor Aerodynamic Design

The main rotor aerodynamic design was performed with an in-house code that uses Blade Element Momentum Theory (BEMT) for both hover and forward flight to calculate the performance of the rotor in terms of Figure of Merit (FM) and cruise lift-to-drag ratio (L/D).The code was validated against R-66 flight test data. The main rotor design geometry prioritized maximizing figure of merit because the wings were designed to carry 80% of the weight in cruise. In hover, the main rotor provides all required lift so high hover efficiency was paramount. The OA212 airfoil provided the highest FM in hover out of the tested airfoils while having a moderate L/D. The final design has a bilinear taper and single linear twist. These parameters, listed in Table 8, create an even α and lift distribution along the blade radius. Main rotor RPM stays constant in both hover and forward flight since the tip velocity of the rotor does not change.

Table 8 Main Rotor Design Details, v_{cruise} = 67.06 m/s (130.35 kts)

Geometry Parameter	Value	Performance Parameter	Value
No.of Blades	5	**Disk Loading**	277.71 N/m^2 (5.8 lb/ft^2)
Aspect Ratio	17	**Power Loading**	49.51 N/kW (8.3 lb/hp)
Radius	5.88 m (19.28 ft)	C_T/σ	0.118
V_{tip}	152.4 m/s (500 ft/s)	**FM**	0.84
Solidity, σ	0.094	M_{tip} @ v_{cruise}	0.455
Main Rotor RPM	247.65 rpm	μ @ v_{cruise}	0.44

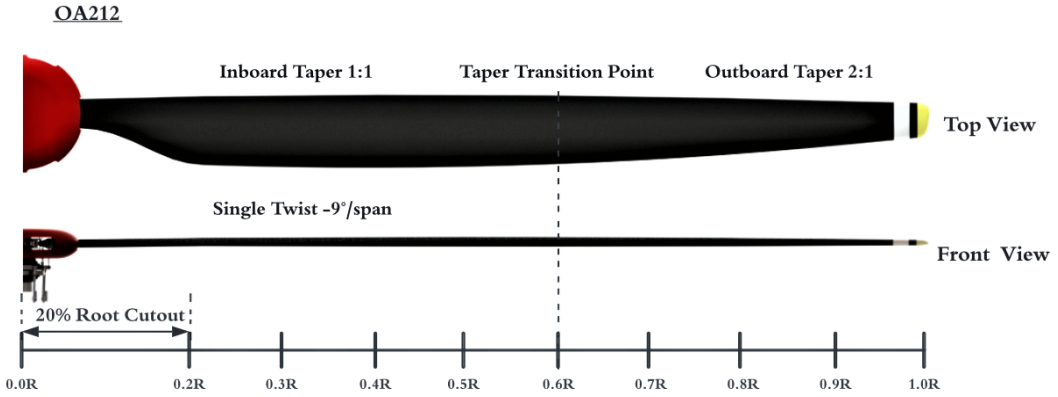

Fig. 14 Main Rotor Blade Geometry

B. Main Rotor Blade Design

The main rotor blade design prioritizes safety, weight, and simplicity of manufacturing. The main load bearing component, the S-Glass D-spar, resists centrifugal forces and bending loads. The spar is filled with Rohacell 51 foam, which is both light, inexpensive, and helps maintain the frontal shape of the rotor blade. The tungsten leading-edge weight assists in locating the center of gravity of the blade at the quarter-chord to help avoid aeroelastic flutter. Lightweight Rohacell 31 foam was chosen to maintain the shape of the rest of the blade and to push the center of gravity further forward.

The blade skin consists of four [±45] plies of T300 graphite/epoxy. The skin provides the majority of the torsional and chordwise stiffness of the blade. Above the skin on the leading edge, a stainless steel erosion guard prevents deterioration of the blade due to the surrounding environment. A thin copper mesh is bonded over the skin to act as grounding in the event of a lightning strike which without it could severely damage the blade skin. An optional deicing strip can also be added to the blade in order to prevent ice build-up, if flying in icy conditions.

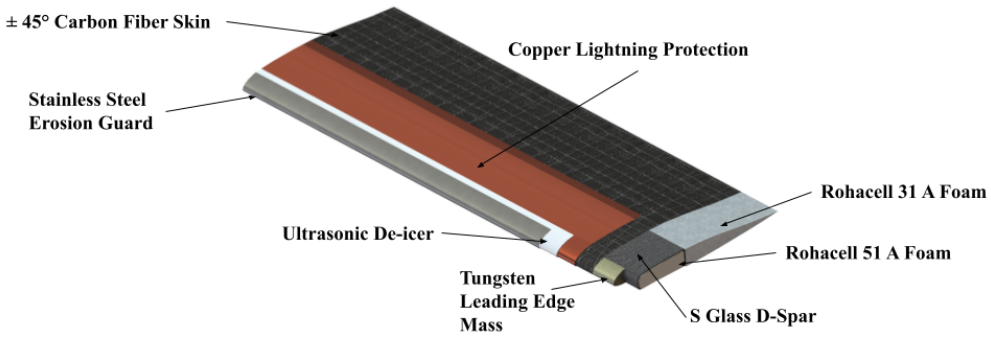

Fig. 15 Blade Structural Composition

C. Main Rotor Hub Design

A key component in determining the main rotor dynamics, as well as Blitzen's stability, vibratory loads, and control characteristics, is the design of the main rotor hub. The main rotor hub transmits torque from the main rotor shaft to the blades and allows lead-lag, flap, and pitch articulation of each individual blade to augment the rotorcraft's thrust vector while reducing transmission of unwanted in-plane and flap moments from the blades to the mast.

Several different types of rotor hub configurations have been successfully demonstrated on helicopters in industry, and each is known for its unique effects on factors from vibratory loads to mechanical complexity. A trade study of 4 types of rotor hub configurations was conducted to set the framework for Blitzen's main hub design: articulated, semi-articulated, hingeless, and bearingless. Teetering hubs were not considered because Blitzen has 5 main rotor blades. A set of main hub design drivers was determined to identify the best hub configuration for Blitzen's mission, as will be discussed later.

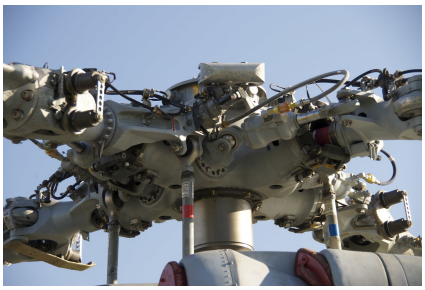

(a) Sikorsky SH-60 Articulated Hub

(b) Bell 407 Semi-articulated Hub

Fig. 16 Articulated and Semi-articulated Hubs

1. Articulated Hubs (Figure 16a)

Articulated hubs use separate mechanical hinges to allow lead-lag and flap articulation and a mechanical bearing to allow pitch articulation. These mechanical hinges and bearings require lubrication, damping, and maintenance. Articulated hubs have relatively low flap hinge offsets and are known for good reduction of hub stresses and vibrations, as well as favorable control authority and gust insensitivity [7]. However, because mechanical hinges and bearings are used for articulation about all 3 axes, they are by far the most mechanically complex configuration. The disadvantages of this hub are high maintenance demands and costs, significant weight (6-7% of GTOW), and complexity.

2. Semi-articulated Hubs (Figure 16b)

Unlike articulated hubs, semi-articulated hubs do not use mechanical hinges or bearings to allow blade articulation about the 3 axes. Instead, a composite flexure provides a virtual flap hinge, and a conical elastomeric bearing allows pitch articulation and movement in the lead-lag plane. Elastomeric bearings consist of several alternating layers of a flexible elastomer and rigid metal alloy and can provide rigidity in some directions and flexibility in others. The elastomeric bearings of semi-articulated hubs are rigid about the flapping axis but flexible about the lead-lag and pitch axes. Unlike mechanical hinges and bearings, elastomeric bearings do not require lubrication systems and only require servicing roughly every 2500 flight hours.

While the initial manufacturing costs of the hub plate flexure and elastomeric bearings may be higher, the reduction in complexity, maintenance needs, and weight provides significant advantages over articulated hubs. Semi-articulated hubs similarly provide good control authority, stability, gust insensitivity, and low vibrations, and they typically contribute to 3-4% of GTOW [7].

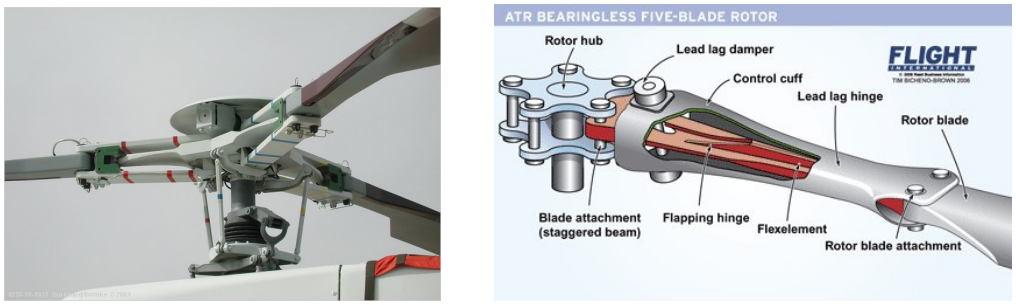

(a) Eurocopter Hingeless Starflex Hub

(b) Eurocopter EC145 Bearingless Hub

Fig. 17 Hingeless and Bearingless Hubs

3. Hingeless Hubs (Figure 17a)

Hingeless hubs are similar to semi-articulated hubs in that they use flexures and elastomeric bearings to achieve articulation about all 3 axes. However, a single flexure provides virtual hinges for both flapping and lead-lag articulation, and elastomeric bearings provide only pitch articulation. Hingeless hubs offer several similar advantages over articulated hubs due to their compact and relatively simple design. They provide relatively good control power, stability, and gust insensitivity, and are low in weight. However, manufacturing costs are greater for flexures that provide virtual hinges about 2 axes, and the stiffer design of hingeless hubs has been known to yield greater vibratory loads.

4. Bearingless Hubs (Figure 17b)

The final configuration studied was the bearingless hub. As the name suggests, this configuration uses virtual hinges and bearings for all blade articulation, achieved through the use of a single flexbeam. The flexbeam is designed to be torsionally soft and can thus twist to allow pitch articulation. The pitch horn extends from a torsionally rigid torque cuff encasing the flexbeam and fixed to the blade attachment, which transmits pitch torque from the pitch links to the blade. Bearingless hubs are very compact, have the fewest parts, and the lowest weight. However, manufacturing costs of the torsionally soft flexbeams is higher, and the requirement of a torque cuff necessitates large root cutouts from lift-producing surfaces near the hub [7]. Additionally, while bearingless hubs have been demonstrated on smaller and medium-sized helicopters, they have yet to be demonstrated on rotorcraft exceeding 5 tons and are still quite uncommon in industry. Bearingless hubs provide advantages including low demand for servicing, high gust insensitivity, and high control authority. However, these come at the expense of greater vibration issues, especially in rotorcraft with high advance ratios above 0.3 [13]. For reference, Blitzen's advance ratio in cruise is 0.44.

5. Hub Configuration Selection

The hub design drivers were based on vibrations, weight, stability, complexity, control power, gust insensitivity, maintenance costs, and manufacturing costs. Table 9 shows the Pugh Matrix used for the rotor hub configuration selection. Design drivers are listed by normalized weight in descending order. Safety and passenger comfort, tied to drivers like stability and vibration reduction, were prioritized, whereas drivers like initial and operating costs were deemed to be of lower priority.

Table 9 Pugh Matrix for Main Rotor Hub Configuration Selection

Design Driver	Driver Weight	Articulated*	Semi-articulated	Hingeless	Bearingless
Vibrations	21.84%	0	0	-1	-2
Weight	17.84%	0	1.5	2	2
Stability	17.80%	0	2	2	2
Complexity	13.73%	0	2	2	3
Control Power	12.11%	0	1	2	1
Gust Insensitivity	9.92%	0	-1	-2	0
Maintenance Costs	4.04%	0	2	2	3
Manufacturing Costs	2.72%	0	-1	-2	-3
Sum	100%	0.000	0.974	0.839	0.849

*Baseline

As shown in the last row of Table 9, the semi-articulated hub had the greatest sum and was thus selected for the main rotor hub design. Specific features of this semi-articulated hub were further developed to cater to higher-priority hub design drivers, as will be discussed further below.

6. Design Features

Figure 18 shows the design of the 5-bladed, semi-articulated main rotor hub. As discussed of semi-articulated hubs, a fiberglass-epoxy composite flexure provides a virtual flap hinge with 4% offset from the mast center, and conical elastomeric bearings allow lead-lag and pitch articulation. The hub features lead-lag dampers to mitigate vibratory loads. Flap limiters prevent over-coning of the blades beyond ±5°. The pitch horns extend from the blade attachments at the location of the elastomeric bearing to prevent pitch and flap moment coupling. Three electrohydrostatic actuators draw from Blitzen's electric power supply to actuate the lower swashplate for collective and cyclic control. A weather-resistant rubber casing protects the spherical swashplate bearing and internal components from weathering and corrosion to reduce maintenance requirements. The compact hub design helps Blitzen maintain an appropriate spatial footprint and, according to FEA mass analysis using SolidWorks, weighs only 52.62 kgs (116 lbs) - 2% of GTOW. Its relatively few parts reduce maintenance needs and minimize possible points of failure. The hub is encased in a fiberglass aerodynamic fairing for significant drag reduction.

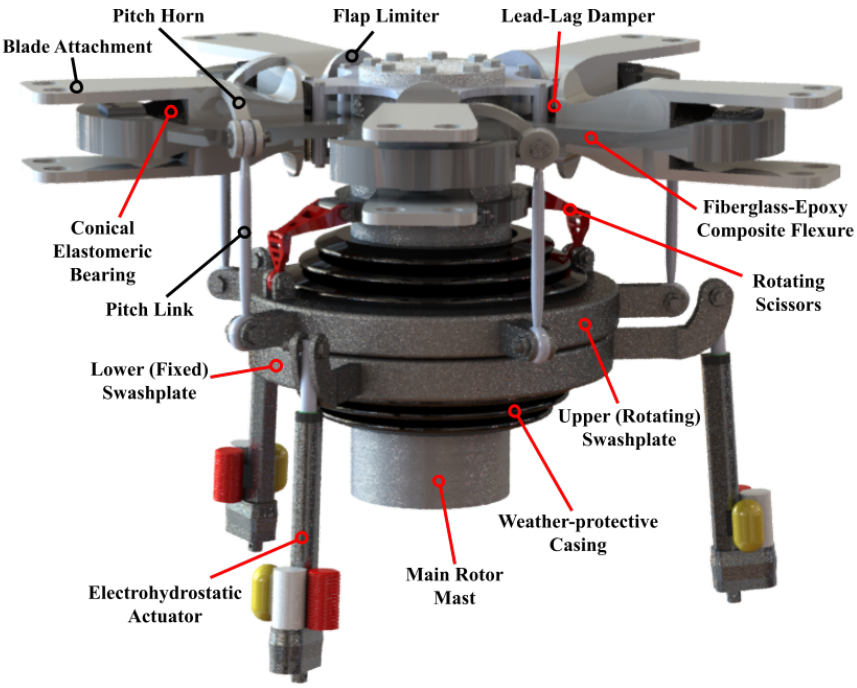

Fig. 18 Semi-articulated Main Rotor Hub

D. Main Rotor Dynamics

The fan plot is shown in Fig. 19 details main rotor flap frequencies. It has been generated using the non-dimensional mass and stiffness distributions for the UH-60A rotor. The non-dimensional flap frequencies at 100% RPM are 1.04, 2.67, and 3.40. The solid colored lines show the 1st, 2nd, and 3rd flapping frequencies for values from 0% to 120% of the operating RPM. The flapping frequencies were calculated by solving for the eigenvalues of the mass-stiffness system matrix using 10 nodes evenly spaced along the blade and assuming uniform stiffness and mass. In the figure it is seen that the second and third flap frequencies are well separated from the rotor-order frequencies.

E. Wing Design

1. Wing Geometry

Blitzen features a high wing to allow space for passenger ingress and egress on the sides of the vehicle. The wing has a wingspan of 9.18 m (30.11 ft) with an aspect ratio of 6.85, which are values set during vehicle sizing; it has an unswept leading edge and a 2:1 taper ratio to concentrate lift near the wing root. The wing is mounted at a 4° angle of attack relative to the fuselage in order to offload lift from the main rotor during the cruise portion of the mission and maximize the lift of the wing. A 3° anhedral was used to avoid interaction with coning of the main rotor.

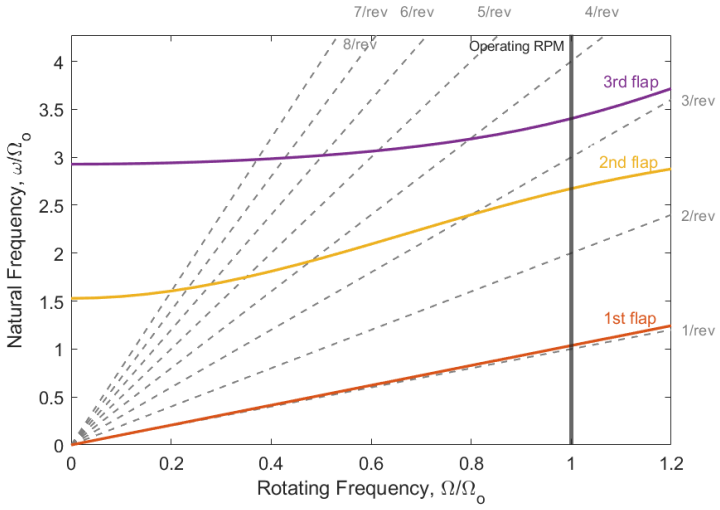

Fig. 19 Fan Plot for the Main Rotor

2. Airfoil Selection

The goal is to choose an airfoil with a high lift coefficient as well as high lift-to-drag ratio since wings carry 80% of the total load in forward cruise flight. Moreover, it is favorable to use a low drag airfoil since cruise propulsive power can be decreased. The low drag NACA 63412 airfoil was chosen for its excellent maximum lift coefficient (C_{lmax}= 1.2) and high lift-to-drag ratio (C_l/C_{dmax}= 77) in the required range of Reynolds number (around $2*10^6$).

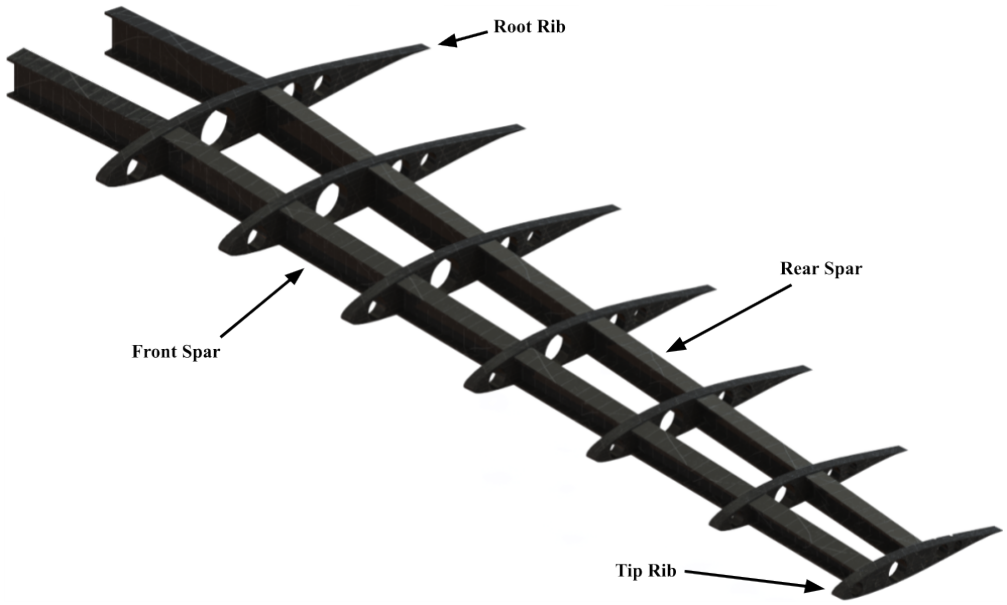

Fig. 20 Wing Structural Design

3. Wing Structural Design

The wing has two I-beam spars located at 20% and 50% of the chord length of 1.68 m (5.52 ft) at root and 0.84 m (2.76 ft) at the tip. The wing structure consists of 7 ribs, evenly spaced every 0.61 m (2 ft) as illustrated in Figure 20.

A carbon/epoxy composite structure was chosen for the spars and ribs because of high fatigue strength in addition to 35% weight reduction compared to a metal equivalent. Each spar and rib is constructed using unidirectional layers of carbon fiber with plies oriented at 0°/90° . The ribs also have 4 layers at 0°/90°. This arrangement helps keep manufacturing relatively simple, while providing required bending stiffness in all axes. There are no ailerons on the wing, as in hover the main rotor and tail rotor provide pitch, roll, and yaw control. During cruise, the main rotor's cyclic actuation supports aircraft pitch and roll control while the rudder addresses the yaw control.

V. Swivel Tail Rotorprop and Empennage Design

A. Swivel Tail Rotorprop Aerodynamic Design

The dual-functional tail rotorprop provides anti-torque in hover and propulsion in forward flight. Transition from anti-torque to thrust compounding mode is performed quickly. The requirement is to design a rotor that would function well both as a tail rotor and as a propeller. A traditional tail rotor uses blades with little to no twist to minimize drag penalties from edgewise flow. Propellers, however, operate in a predominantly axial flow field and are highly twisted to maximize their propulsive efficiency. Blitzen's swivel tail configuration accomplishes both roles. It provides adequate anti-torque and directional control in low airspeed regimes and serves as an effective pusher propeller in forward flight. Additionally, since a majority of the mission profile is cruise, the emphasis was on maximizing propeller efficiency and minimizing the penalties inherent in tail rotor-oriented design at 67.06 m/s (130.35 kts) cruise. Table 10 and Figure 21 show swivel aerodynamic design in detail.

A moderate built-in twist angle of -30.4 deg was chosen since high twist angles would result in rotorprop blade stall the anti-torque configuration. The Clark-Y airfoil was selected since it exhibits high efficiency in terms of Figure of Merit (FM) at low pitch settings. The dimension of 1.52 m (5 ft) diameter was computed using the in-house sizing code. The rotorprop is attached to the swivel gearbox and is located on the vehicle longitudinal axis. The 0.76 m (2.5 ft) radius allows for sufficient ground clearance in both swivel configurations because the rotorprop shaft is 2.233 m (7.3 ft) vertically from the ground.

Table 10 Swiveling Tail Rotorprop Design Details

Geometry Parameter	Value	Performance Parameter	Value
No. Blades	4	**Power**	123.5 kW (165 Hp)
Aspect Ratio	5.08	**Torque @ v_{cruise}**	507.04 N-m (373.97 lb-ft)
Radius	1.52 m (2.5 ft)	**M_{tip} @ v_{cruise}**	0.52
V_{tip}	176.78 m/s (580 ft/s)	**J @ v_{cruise}**	1.191
Solidity, σ	0.251	**η_p @ v_{cruise}**	0.845
Tail Rotorprop RPM	2214 rpm	**Θ_{75} @ v_{cruise}**	12.56 ^{o}

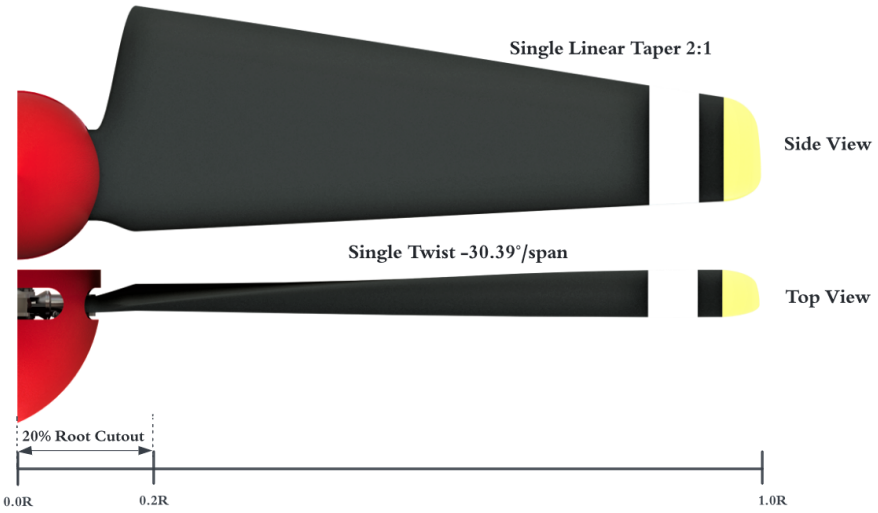

Fig. 21 Swiveling Tail Rotorprop Blade Geometry

B. Swivel Tail Rotorprop Structural Design

A composite design was selected for the swivel rotorprop to reduce system weight and ease transition between its two modes. The rotorprop has two primary sections: the blade attachment and the blade. The blade attachment is a

metallic connection, which helps transmit the centrifugal and bending loads from the blade to the hub and assists in actuation for propeller and rotor control.

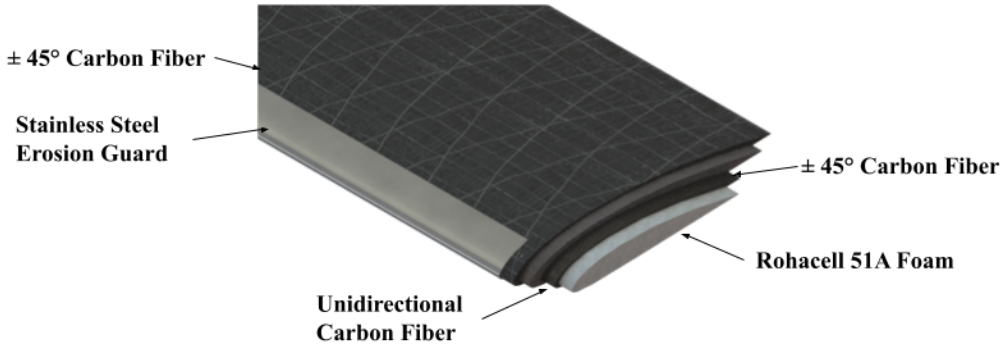

Fig. 22 Swivel Tail Rotorprop Structural Composition

The blade consists of six main components; a Rohacell 51A foam core, a ±45° carbon fiber wrap, an graphite/epoxy unidirectional spar, an outside ±45° carbon fiber wrap, an erosion strip, lightning protection, and optional de-icing technology. Bending, lag, and centrifugal loads are all carried by the unidirectional spar, while the ±45° wraps provide a majority of the torsional stiffness. A stainless steel erosion shield similar to the one used on the main rotor blade is bonded to the leading edge to protect from any deterioration due to debris. Additionally, a copper mesh and de-icing strip are mounted over the skin similar to the main rotor design.

C. Rotorprop Hub

Figure 23 shows the design of the 4-bladed rotorprop hub. It is rigid in-plane and in flapping and features thrust bearings to support blade retention and collective pitch articulation. The yellow spider above the hub transmits collective pitch control to each of the blades via four steel pitch links. A single electrohydrostatic actuator provides collective control to the spider via a rod inside of the hollow tail rotor shaft. The rigid, compact rotorprop hub design allows for safe anti-torque in the hover configuration while maximizing thrust and control in cruise configuration.

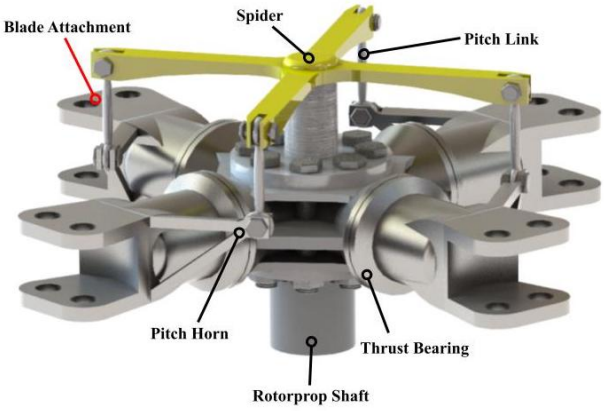

Fig. 23 Rotorprop Hub

D. Vertical Stabilizer Design

The NACA 63418 low drag airfoil was chosen for the vertical stabilizer. The thicker chord span ratio of this airfoil relative to the wing provides additional space for rotorprop housing and rudder actuation system structural elements. Using this airfoil at an angle of incidence of 4°, a planform area of $0.808m^2$ is required to counteract the main rotor's 9500 Nm (7007 ft-lb) of torque at cruise velocity. The required planform was determined under the assumption that the area taken up by the swivel-mechanism casing would not contribute to or impede the resulting countertorque. In order to transition the rotorprop from tail rotor to pusher propeller mode before reaching cruise velocity, a rudder is included in the vertical stabilizer. The rudder controls vehicle yaw while in cruise, as the rotorprop is a pusher propeller during this flight phase.

E. Horizontal Stabilizer Design

The horizontal stabilizer counteracts pitching moments induced by the fuselage in cruise. The stabilizer was sized using empirical data [7] informing Equation (3). The equation results in a 0.935 m^2 (10.06 ft^2) planform area. A NACA 63412 low drag airfoil was selected to provide necessary lift at a small angle of incidence while minimizing drag penalties caused by thickness.

$$S_h = 0.0086\pi R_{MR}^2 \tag{3}$$

VI. Vehicle Performance

A. Equivalent Flat Plate Area Estimation

Blitzen's mission profile is dominated in time and distance by the cruise segment. Thus, an accurate representation of vehicle drag in this flight regime is critical to properly estimate vehicle performance. A team-developed code was created to calculate equivalent flat plate area of the fuselage. The fuselage was discretized into sections (i) that were modeled as cylinders. Form Factor (FF), Skin Friction Coefficient (C_f), and fuselage flat plate area (f) were then obtained for each section using the following equations from Hoerner [14].

$$FF_i = \frac{C_{D,wet}}{C_f} = 1 + 1.5(d/l)^{\frac{3}{2}} + 7(d/l)^3 \tag{4}$$

$$C_{fi,t} = \frac{1.328}{\sqrt{Re}}(1-p) + \frac{0.455}{(\log_{10} Re)^(2.58)(1+0.144M^2)^{0.65}}(p) \tag{5}$$

$$f = C_{D0}S_{ref} = \sum_{i=1}^{N} IF_i C_{fi} FF_i S_{wet,i} \tag{6}$$

Here, d/l is the fuselage fineness ratio and p is the percentage of the aircraft skin experiencing turbulent flow. p was set to 0.65, as a well designed composite-body aircraft may experience laminar flow over up to 35% of the aircraft surface [15]. S_{wet} is the wetted area of a single discretized fuselage segment obtained from the vehicle CAD and IF is an interference factor used to model drag from component attachment points to the main fuselage. This estimation computes f to be 0.67 m^2 (7.2 ft^2), consistent with the flat plate area used during vehicle sizing.

B. Hover Download Estimation

An accurate estimation of hover download is required because the rotor wake impinges on Blitzen's wing significantly more than on the fuselage of a conventional helicopter.

$$\Delta D_{vn} = \int_{x_n}^{x_n+\Delta x_n} C_{Dvn} q_n w_n \, dx \tag{7}$$

Equation (7) was used to estimate download in hover. The rotorcraft was discretized into segments from a top-down view to calculate total download factor as a sum of download contribution from segments. C_{DV} ranged between 0.4-1.2 with the fuselage sections having the lowest value and the wing having the highest [7]. The fuselage was designed to minimize C_{DV} since the wing was expected to cause significant download. Blitzen's download is calculated to be 17.2% of its GTOW, 1.2% higher than the expected download during sizing. This difference was deemed acceptable, as the propulsion system is capable of continuously providing 5.5% more power than is required for the highest power mission segment.

C. Vehicle Performace Metrics

Flight power requirements were computed using aerodynamic parameters and standard energy methods [7]. Rotor wake download and thrust informed main rotor power while equivalent flat plate area, wing induced drag, and wing profile drag characterized pusher propeller power. Figure 24(a, b, c) illustrates required power for the two sets of motors installed in the Blitzen (main rotor and rotorprop) against flight velocity. OGE hover is possible with one motor inoperative (OMI) out of the six powering the MR. Forward flight at full cruise velocity is possible with OMI out of the four rotorprop motors.

The velocity for best range (V_{br}) is 49.72 m/s (96.65 kts). Cruise velocity for best endurance (V_{be}) is 43.62 m/s (84.8 kts). However, Blitzen is capable of cruising at 77.17 m/s (150 kts) with its nominal cruise speed set to 67.06 m/s (130.35 kts). These velocities were computed at a cruise conditions of 1219 m (4000 ft) MSL and ISA+20C.

As shown in Figure 24d, Blitzen is capable of flying the entire cruise distance of 148.9 km (92.4 mi) in ISA+20C conditions at 1219 m (4000 ft) MSL with a maximum payload of 544.3 kg (1200 lbs). Further ranges can be achieved with fewer passengers and less luggage weight. Additionally, lower ambient temperatures improve available cruise range. Maximum cruise range also increases if forward flight velocity decreases from the nominal cruise speed to V_{br}.

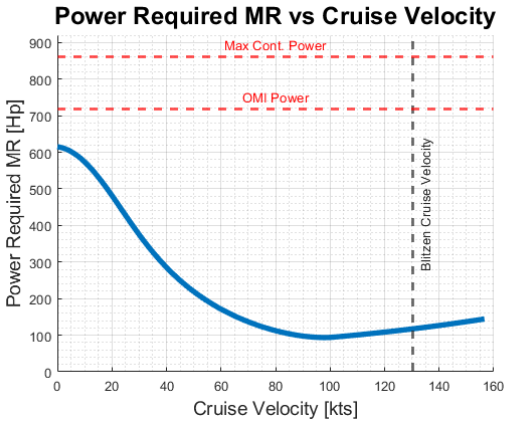

(a) MR Power vs Velocity

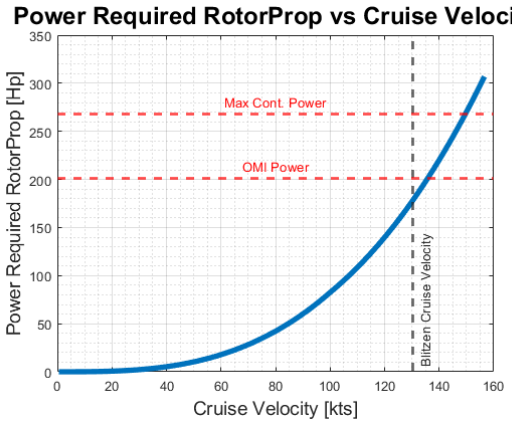

(b) Rotorprop Power vs Velocity

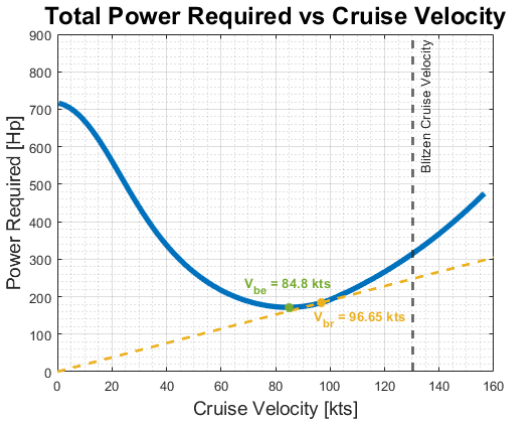

(c) Total Vehicle Power vs Velocity

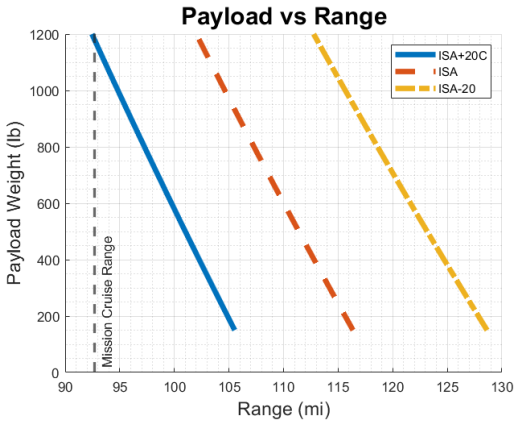

(d) Variation of Allowable Payload with Range

Fig. 24 Flight Performance Metrics

VII. Propulsion and Transmission

Based on the RFP, Blitzen is designed to be an electric VTOL vehicle or eVTOL. Initial sizing done by the Aerodynamics team calculated main rotor installed power to be 535.14 kW (462.58 hp). This is accomplished using electric motors.

A. Desirable Characteristics

Some of the more desirable characteristics when choosing a motor for eVTOL use is a high specific power (kW/kg). High efficiency over a wide range of RPMs with constant torque and power output is another desirable characteristic. Motor cost and fault tolerance are large considerations during motor selection. Exceptional fault tolerance is desirable so that minor manufacturing defects in the motor will not cause catastrophic damage during flight.

B. Motor Types

Electric motors can be categorized by input power supply types (Figure 25) [7]. Each motor type can have a variety of different uses, such as the stepper motor being used in Computer Numerical Control (CNC) machines for quick and precise movement, to brushed DC motors being used in model train sets. AC induction motors see a wide use due to their relatively maintenance free life span, resulting from a lack of brushes, commutators, or slip rings, which can easily degrade over time.

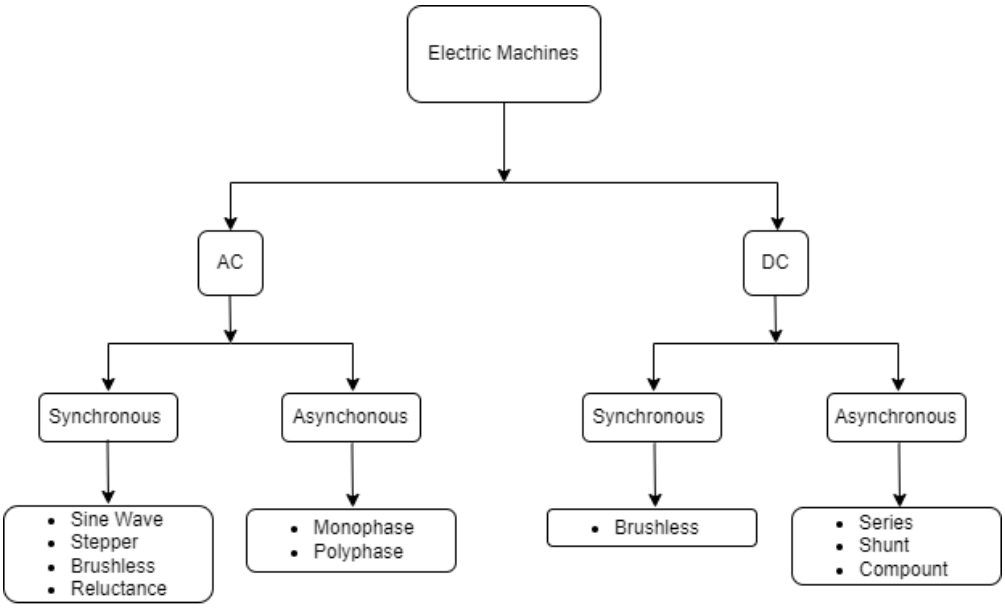

Fig. 25 Types of Motors

C. Motor Selection

A study of over fifteen different motors was conducted, ranging from AC induction motors to axial flux motors (Table 11). Motor selection for Blitzen was carried out with power output and weight in mind. Most electric motors studied have a relatively high efficiency over a wide range of RPM and torque. The study was narrowed to seven motors from the motors studied. These motors were compared by their weights, peak and continuous power outputs, peak and continuous torque output, and geometry (Table 11).From this table the EMRAX type axial flux motor was chosen because of its high specific power.

Table 11 Motors and Their Compared Characteristics

Motors	Yaza 750R	TGO-190	TGO-715	AFM 240	Yaza P400R	EMRAX 268	EMRAX 228
Mass [**kg**] (lbs)	**37** (81.6)	**3.3** (7.2)	**2.7** (5.9)	**80** (176.4)	**28.2** (62.2)	**20** (44.1)	**12** (26.5)
Aspect Ratio	4	4.1	4.7	1.8	2.1	3.0	2.7
Through Shaft [**mm**] (in)	**52** (2.04)	**159** (6.27)	**161** (6.34)	NA	NA	**57.15** (2.25)	**38.1** (1.5)
Peak Torque [**Nm**] (ft-lbs)	**790** (583)	**40.8** (30.02)	**23.25** (17.14)	**800** (590)	**370** (273)	**500** (369)	**230** (170)
Peak Power [**kW**] (hp)	**200** (268.2)	**25.6** (34.4)	NA	**335** (476)	**160** (214.5)	**200** (268.2)	**109** (146.2)
Cont. Torque [**Nm**] (ft-lbs)	**400** (295)	**9.46** (7.0)	**4.83** (3.56)	**440** (325)	**200** (147.5)	**200** (147.5)	**96** (70.8)
Cont. Power [**kW**] (hp)	**70** (94)	**5.9** (8)	**4.04** (5.4)	**150** (201)	**60** (80.5)	**86** (115.3)	**50** (67.1)
Specific Power [**kW/kg**] (hp/lbs)	**5.4** (3.3)	**7.8** (4.8)	NA	**4.2** (2.7)	**5.7** (3.4)	**10** (6.1)	**9.1** (5.5)

D. EMRAX Motors

EMRAX motors are a type of axial flux motor that have a high power output while remaining light and small. EMRAX motors can be customized in three variants: low voltage with a maximum battery voltage of 250 Vdc and a max motor current of 1000Arms, medium voltage with a maximum battery voltage of 650Vdc and maximum motor current of 400Arms, and high voltage with a maximum battery voltage of 800Vdc and a maximum motor current of 250Arms, for the EMRAX 268. These motors also come with three different options for cooling, the first being completely air cooled with an airflow of 20m/s (44.74 mph) at a temperature of 25 °C (77 °F). The second is completely liquid cooled with a water/glycol flow of 8L/mi at 25 °C (77 °F). The last cooling option is combo-cooled, which is a combination of both air cooling and liquid cooling [3].

These motors have been specifically designed with through-shaft capability, allowing multiple motors to be placed and mounted on the same axle, potentially doubling or tripling the power output on a single shaft. Because of the "through-shaft" design, these motors output a tremendous amount of power while taking up a small amount of space. [3]

1. EMRAX 268

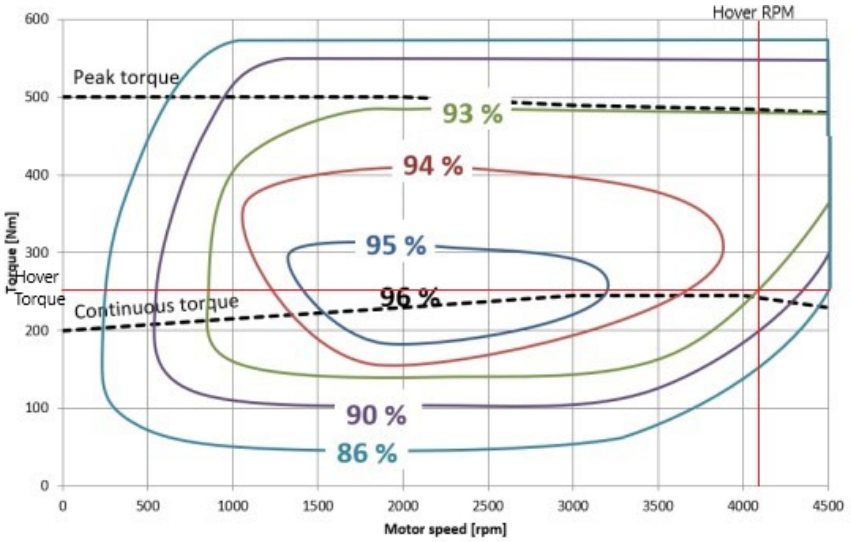

Fig. 26 Efficiency map of the EMRAX 268 Motor [3]

The EMRAX 268 can provide a maximum power of 200 kW (268.2 hp) at 4500 RPM, and a continuous power of 107 kW (143.5 hp) with specific cooling options. The EMRAX 268 can also provide a peak torque of 500 Nm (368.8 ft-lbs) and a continuous torque of 250 Nm (184.4 ft-lbs) with a very high efficiency between 90% - 96% (Figure 26). Running the EMRAX 268 at medium voltage with the combo cooling option, with a nominal continuous torque output of 250 Nm (184.4 ft-lbs) and output power of 107 Kw (143.5 hp), gives a motor speed of 4087.40 RPM using Equation (8) [3].

$$\textbf{Power} = \frac{N * \tau}{9550} \tag{8}$$

Here, N = RPM and τ = Torque in N-m. At a torque output of 250 Nm (184.4 ft-lbs) and a motor speed of 4087.40 RPM gives a motor efficiency of 93% (Figure 26).
These motors present a very lightweight and high power option for Blitzen's main rotor power plant.

2. EMRAX 228

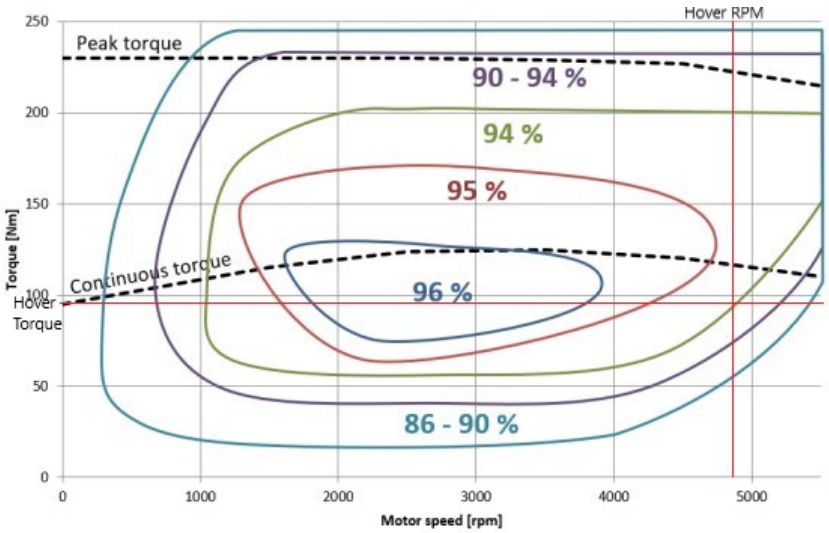

Fig. 27 Efficiency map of EMRAX 228 motor [3]

The EMRAX 228 is much like the EMRAX 268 with the only difference being diameter and power output. The EMRAX 228 possesses the same "Through-shaft" technology as the 268, allowing multiple motors to be mounted onto the same shaft, increasing power output while saving space. Using Equation (8) for power, torque, and speed, and with a nominal torque output of 96 Nm (70.8 ft-lbs) providing a continuous power of 50 kW (67.05 hp) gives a speed of 4973.96 RPM. At a torque output of 96 Nm (70.8 ft-lbs) and a speed of 4973.96 RPM, the motor efficiency is 94% (Figure 27).
The through-shaft capability, low weight, and high power output of these motors are excellent characteristics for the tail rotorprop.

E. Controllers and Servos

The controllers used for the main rotor motors is the Unitek Bamocar D3 700 200/400. The rotorprop motors use the Unitek Bamocar D3 200/400 controller. The RFP states that in the vehicle should be able to complete its required mission with a single power system failure. Blitzen uses one motor controller per motor, ensuring that the aircraf twill be able to complete its mission in the event of a single motor controller failure.

Blitzen needs to have stepper motors to move the tail rotorprop from its position in hover mode to its position in cruise mode due to the need for accurate and low RPM movement. The NEMA 34 motor provides a high holding torque of 4.8 Nm (3.5 ft-lbs) with a relatively light weight of 5.3 kg (11.7 lbs) each. For redundancy Blitzen will run two of these stepper motors for its tail mechanism.

F. Motors Conclusion

The EMRAX 268 and 228 are the ideal motors to power all rotors on the vehicle. Specifically, the EMRAX 228 being used for the tail rotorprop running at 4973.96 RPM with an efficiency of 94%, and the EMRAX 268 being used for the main rotor running at 4087.40 RPM at an efficiency of 93%. Blitzen will use four of the EMRAX 228 motors to reach the required power output in the tail rotorprop; it will also use six EMRAX 268 motors for the main rotor.

Table 12 EMRAX Characteristics

Motors	EMRAX 228	EMRAX268
Diameter [**mm**] (in)	**228** (8.96)	**268** (10.6)
Width [**mm**] (in)	**86** (3.4)	**91** (3.6)
Weight [**kg**] (lbs)	**12** (26.5)	**20** (44.1)
Peak Torque [**Nm**] (ft-lbs)	**230** (170)	**500** (369)
Peak power [**kW**] (hp)	**109** (149.2)	**200** (268.2)
Cont. Torque [**Nm**] (ft-lbs)	**96** (70.8)	**200** (147.5)
Cont. Power [**kW**] (hp)	**50** (67.1)	**86** (116.3)

G. Main Rotor Gearbox

Table 13 Main Gearbox Weight, Tooth, Ratio and RPM Breakdown

Part	**Weight (AISI 9310 Steel)**	**Tooth Count**	**Ratio**	**RPM**
Input Pinions	.22 kg (.48 lbs) each	25	-	4087.40
Straight Bevel Gear	4.11 kg (9.05 lbs)	103	4.12	992.09
Planetary Set	6.35 kg (14.00 lbs)	34 (sun and 3 planets), 102 (ring)	4	248
Shafts and Connections	8.30 kg (18.29 lbs)	-	-	-
Totals	**19.19 kg (42.3 lbs)**	**366**	**16.48**	**-**

1. Main Gearbox Description

The main rotor gearbox ultimately has the purpose of reducing the RPM of the electric motors to that which is required for hover and forward flight of the main rotor. The RPM incoming from the motors is 4087.40 RPM, whereas the main rotor blades are spinning at 248 RPM. This leads to a reduction ratio of 16.48, which is a ratio of the input RPM to the output RPM. The rated torque of the motors is 1500 N-m (1106.34 lb-ft). A reduction ratio of 16.5 means that the output torque from the gearbox will be 24,750 N-m (18,254 lb-ft), which is about 24% higher than the torque required for hover. A summary of key characteristics for each step in the gearbox can be found in Table 13.

The configuration chosen for the Blitzen is a simple 2-stage design that prioritizes efficiency and compactness, as shown in Figure 28. Each stage features a reduction ratio of about 4, which allows for an even distribution of the forces and vibrations throughout the system. When sizing the gears in the gearbox, it was also important to make sure that the

gears were sized relative to each other, the shaft connections, and the size of the helicopter as a whole. For example, if one gear is double or triple the size of another gear, it makes for an awkwardly shaped gearbox, which leads to an awkwardly shaped case. Changing the pitch diameter of the gear teeth is a simple method to change the size of the gears without affecting the achievable reduction ratio.

The first stage consists of a pinion and a straight bevel gear, which reduces the RPM of the motors by 4.12. Straight bevel gears are needed because of the directional change between the motor shaft and the main rotor shaft. Straight bevel gears are also significantly easier and cost effective to manufacture than helical bevel gears, so they were chosen for this configuration.

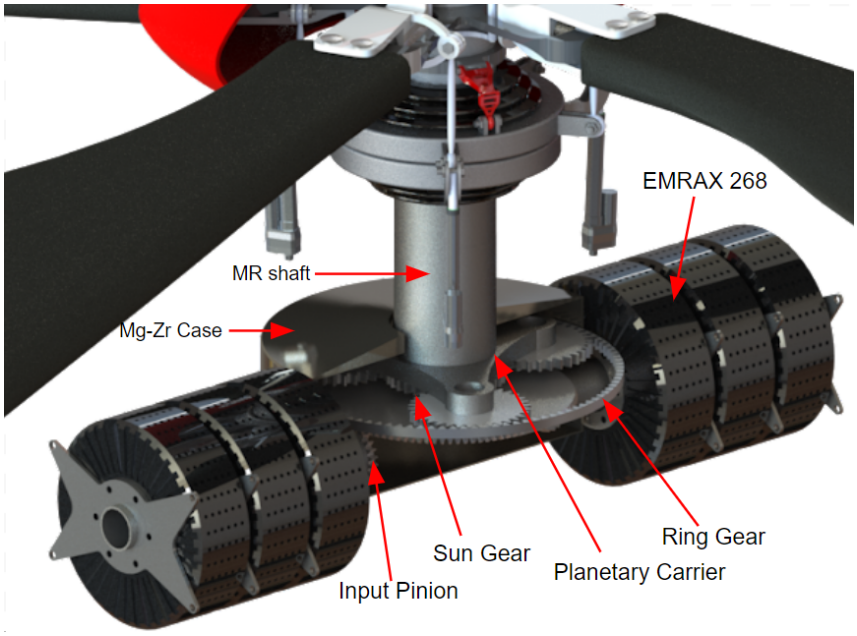

Fig. 28 Main Rotor Gearbox

The second stage consists of a planetary gear set, which is common practice in most helicopter configurations. Planetary gear sets consist of a sun, ring, and planetary carrier gear. Planetary gears take up very little vertical space, which is already limited above the passengers in Blitzen's configuration where the main gearbox will be. Additionally, planetary sets create significantly less noise than other transmission types because of the increased amount of teeth in contact. In a planetary gear set, one of the 3 components (sun, ring, planetary carriers) must be fixed so that the other two can rotate around the fixed component. For calculating the reduction ratio of a planetary gear system, the following equations can be utilized:

$$N_{PlanetaryCarrier} = N_{Sun} + N_{Ring} \tag{9}$$

$$R.R._{planetary} = \frac{N_{PlanetaryCarrier}}{N_{Sun}} \tag{10}$$

where N_{gear} corresponds to the tooth counts of a specific component. For a planetary gear set, the caveat as opposed to calculating a traditional gear ratio is to sum the sun and ring tooth counts to get the tooth count of the planetary carrier.

2. Gearbox Materials and Lubrication

All gears, pinions, and shaft connections will be made out of AISI 9310 steel, which has a density of 7800 kg/m^3 (486.94 $slugs/ft^3$). AISI 9310 was chosen because of its prevalence in current helicopter transmission systems. AISI 9310 has reliable durability for high operational speeds, and the material strength required to prevent wear. The cylindrical casing of the gearbox, which is used to mount to the bulkheads of the helicopter, is made out of Magnesium Zirconium. This material is also commonly used for helicopter gearbox casings, due to its light weight and resistance to corrosion.

MIL-PRF-23699 lubrication oil is used in the gearbox. Additionally, six oil injectors are positioned around the gearbox to ensure a complete lubrication of all gears and connections. Two injectors are placed at the top and bottom faces of the casing and the other four are evenly dispersed around the inner wall of the casing. Due to the circular nature of the casing, these 4 injectors can be 90 degrees apart.

H. Rear-Mounted Swiveling Rotorprop Mechanism

1. Swivel Mechanism Description

The rotor swiveling mechanism, labeled as a "rotorprop", doubles as a tail rotor in hover and a propeller in forward flight, as shown in Figure 29. To achieve this, a 90 degree "swivel" is necessary to adapt to forward flight from hover, or vice versa. Powered by two stepper motors, the swivel casing sits on top of a large spur gear which completes the 90 degree rotation.

The casing moves independently of tail rotor rotation, so the mechanism can transition between the modes while still providing anti-torque or forward propulsive force, which is important for a smooth transition between the two modes. This is done by fitting a bearing between the connection of the tail rotor shaft and the swivel mechanism casing, which allows for rotation and the transfer of torque to spin the mechanism.

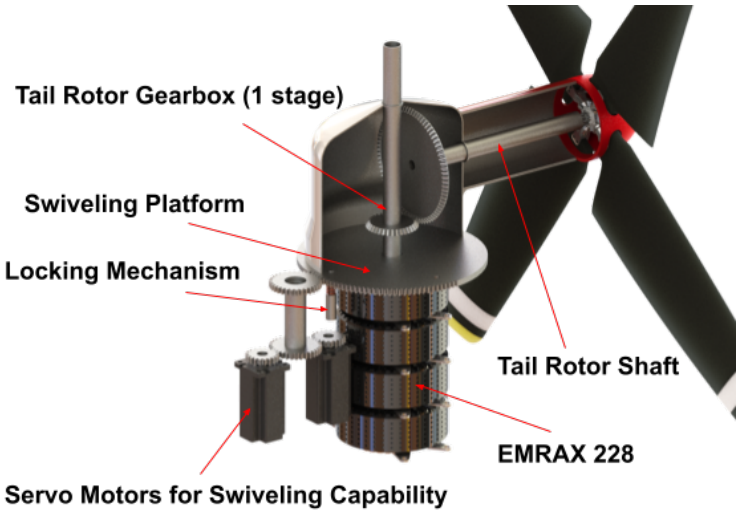

Fig. 29 Swiveling Rotor

Inside of the swivel casing is a straight bevel gear set with a reduction ratio of 2.25:1, which is a small enough ratio to complete in one reduction stage, meaning that the directional change and RPM reduction can be done in a very simple design. The casing covering the gears leading to the tail rotor are contained in an elliptical casing, since they will be sitting on the outside of the fuselage. The elliptical shape will help to reduce the drag of the mechanism in forward flight, while providing protection from the elements and other external forces.

As with the main rotor gearbox, all gears and connections will be made out of AISI 9310 Steel. Additionally, the large gear which supports the swivel casing only needs teeth around 1/4 of the outer surface to support the 90 degree swivel movement. This will reduce manufacturing and cost requirements without sacrificing functionality.

2. Locking Mechanism

A locking mechanism is required for the rotorprop to ensure reliable operation despite external forces, such as wind, to prevent unintentional divergence from either anti-torque or pusher propeller mode. The locking mechanism will consist of a electromagnetically powered solenoid, which can engage in the swivel mechanism in either the tail rotor or propeller mode. This locking mechanism has a pin that can fit through a hole in the gear carrying the swivel mechanism, forcing the swivel system to be fixed in one position when needed.

VIII. Battery System

One of the main challenges of designing Blitzen was utilization of a battery to provide all required energy for a long-range eVTOL mission. The RFP requires that electrical power is provided by a battery with an energy density of 400 Wh/kg (0.243 hp-hr/lb). This energy density has not been demonstrated in current battery technology for aircraft. However, to estimate the volumetric density for Blitzen's battery pack consistent with current battery technology, a calculation was performed based on existing and developing batteries utilized in various industries. The procedure for selecting the battery pack sufficient for aircraft consisted of comparison of the chemistry, configurations (cylindrical, pouch, or prismatic), and various cells from different industries. The trend-line of the current and near-future battery technology, and sizing the battery pack is obtained using this analysis.

A. Battery Selection

To find the most desirable battery system for the vehicle, a comparison of chemistries, configurations, and batteries under development for future use was conducted.

Minimization of battery weight was more crucial for Blitzen over fuel-powered VTOL aircraft due to the battery being a significantly larger portion of vehicle GTOW than fuel.

1. Battery Chemistry

There are numerous battery chemistries currently used in various industries. Lead-acid, Nickel Cadmium (NiCd), Nickel-metal hydride (NiMH), lithium-ion, and lithium are the most widely used chemistries. Since each battery chemistry has a unique energy density and reactionary behavior, their use varies widely. Lead-acid, NiCd, and NiMH batteries are low-cost and widely used batteries but are not sufficient for producing power for eVTOL aircraft. The lead-acid battery has a characteristic where its capacity decreases when high power is discharged. NiCd batteries are being phased out of use due to a low energy density and memory effect, therefore, NiMH batteries are used as replacements. NiMH batteries are not typically recharged after use and must be replaced after discharge. Additionally, these batteries do not have a high enough energy density to produce energy for a long range eVTOL. Lithium-ion batteries are a widely used due to their high energy density compared to NiMH batteries and available safety features. One of the important aspects of the Lithium-ion battery is that it is rechargeable using a charger equipped with cell monitoring and automatic full-charge power shutoff. This battery chemistry requires minimal supervision and provides a greater energy density than older battery types. Thus, this battery is widely used in vehicles, power tools, and portable electronic devices.

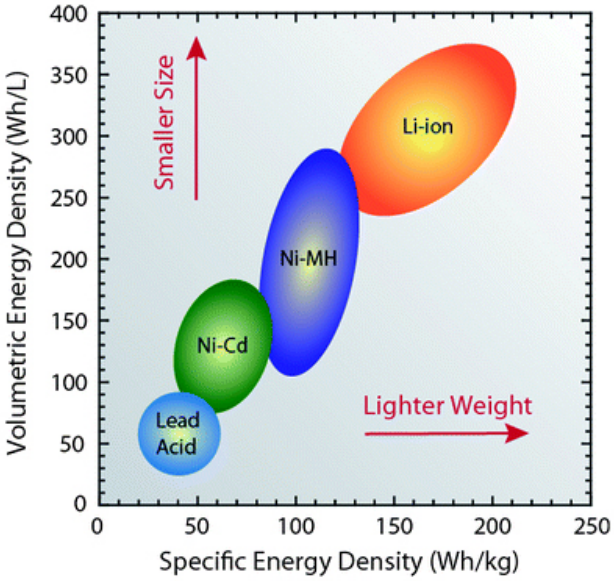

Fig. 30 Chemistry Energy Density [4]

The solid-state battery a novel battery technology that uses a solid electrolyte instead of a liquid to store energy. It provides a low risk of explosion or fire and has a higher energy density than Li-ion batteries. However, this battery is still under development and listed as TRL (Technology Readiness Level) 3 which is defined as experimental proof-of-concept [16]. Therefore, the solid-state battery is in the initial phase of laboratory studies, and is not yet safe enough to be implemented for the aircraft. Considering multiple different chemistries, the most qualifying battery chemistry for the eVTOL aircraft is the lithium-ion battery. Li-ion battery is commonly utilized for electric vehicles and other high-energy requiring systems due its high energy density.

2. Cell Configuration

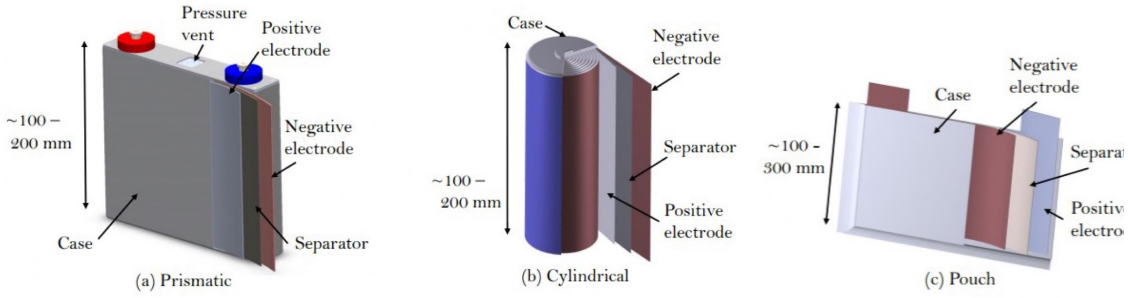

Fig. 31 Various Cell Configurations [5]

The three most common configurations of batteries are: prismatic, pouch, and cylindrical, shown in Figure 31. Different configurations have different characteristics where ones more vulnerable than the other. Cell configuration design drivers were developed and weighed against one another to select the most qualifying cell type for the aircraft. Table 14 details the Pugh Matrix comparison between the three configurations in reference to the design drivers. The cylindrical battery scored highest in the Pugh Matrix and will be used in the aircraft. The cylindrical cell is highly

popular due to to its stable, safe to use, inexpensive, and uniform characteristics. One disadvantage of this configuration is packing density. Unlike prismatic and pouch configurations, cylindrical creates a gap between each cell in a battery pack. However, the high stability and low damage vulnerability aspect of the cell is deemed more important since it is closely related to safety of the aircraft.

Table 14 Battery Configuration Pugh Matrix

	Cylindrical	Prismatic	Pouch
Manufacturing	3	2	1
Weight	2	3	1
Vulunerability	3	1	2
Stability	3	2	1
Cost Efficiency	3	1	2
Packing Density	1	2	3
Total	15	11	10

3. Battery Trend-line [1] [2]

The RFP states that the mass density for the battery pack(s) shall be based on current battery technology. To establish the mass density that is the best fit for the ideal cell of 400 Wh/kg (0.243 hp-hr/lb), data points for various widely-used high-density batteries from multiple manufacturers were obtained to create trend-line. From Figure 32, at 400 Wh/kg specific energy, volumetric energy density is in the 760 to 780 Wh/L or 28.84 to 29.61 hp-hr/cubic ft. range. Since current battery technology varies in volumetric energy density, collecting numerous data points ensures an accurate trend-line to extrapolate the volumetric density of Blitzen's battery.

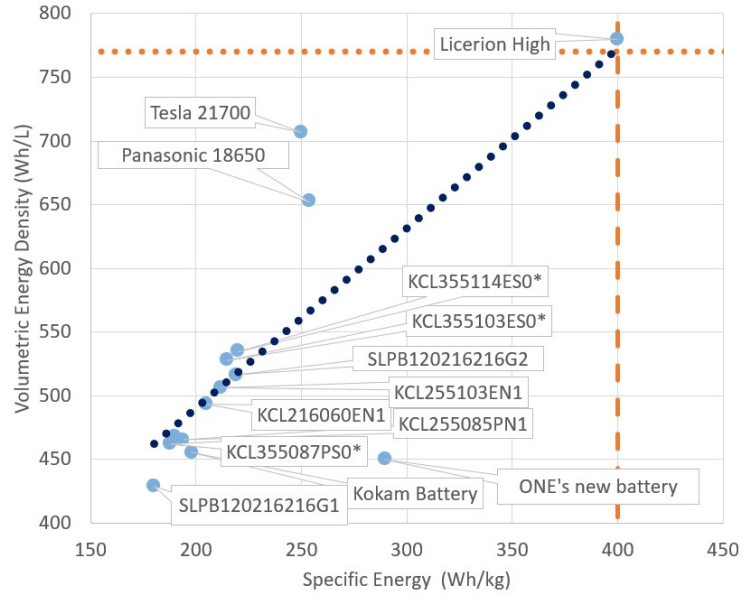

Fig. 32 Battery Trend-line

B. Battery Sizing

According to Section III, Blitzen requires a total of 287000 Whr (384.9 hphr) stored in the batteries for flight. This includes the 20 minute cruise additional reserve power as requested by the RFP and additional 10% for the control electronics and power loss from the motor efficiency. Using the idealized battery with an energy density of 400Wh/kg, the battery pack weighs 720 kg or 1585.7lb. Additionally, from the trend-line from Figure 32 comparing specific energy with volumetric energy density, the volumetric energy density is estimated in 770Whr/L. Using this, the volume of the entire battery will be 0.38 cubic m or 13.40 cubic ft. Each battery pack is 2.24 cubic ft. Figure 33 illustrates battery positioning in the rotorcraft.

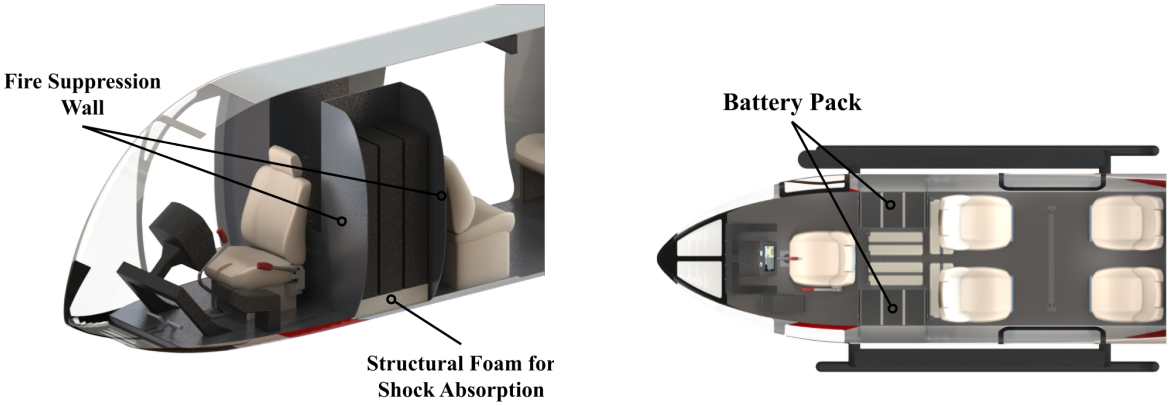

(a) Battery Isometric View **(b) Battery Top View**

Fig. 33 Battery CAD

1. Battery Pack Selection

The number of battery packs was selected based on operational redundancy to allow for safe continuation of the mission with a single battery failure. Use of more battery packs reduces energy loss due to single battery failure, however, battery weight increase from more wiring and casing. Therefore, Blitzen's battery was separated into six packs. Further analysis on number of packs selected is in Section XV.B of this report.

2. Battery Sizing Calculation

To accommodate motor voltage and current requirements, individual cylindrical cells were placed in series and parallel configurations within a battery pack. SAMSUNG INR21700 battery packs, with 3.6V and 3.9Ahr, are placed in series and parallel patterns in accordance to the EMRAX 268 motor requirements of 700VDC and 200A. This battery was used to represent the realistic number of the battery cells used with current battery. The calculation is shown below.

$$N_{series} = \frac{V_{motor}}{V_{cells}} = \frac{700}{3.6} = 194.44 \tag{11}$$

$$N_{parallel} = \frac{Q_{motor}}{Q_{cells}} = \frac{200}{3.9} = 51.68 \tag{12}$$

$$N_{batteries} = 195 * 52 = 10140 \tag{13}$$

Equations 11 and 12 shows 195 cells in series and 52 cells in parallel are required to run the EMRAX 268. Equation 13 shows the total number of cells that are required. Blitzen also utilizes the EMRAX 228 motor, requiring 600 VDC and 180 A. A DC to DC step-down voltage converter is included to accommodate for the tail motors at 600 V. There are six packs of batteries, so total energy is distributed into six parts. Each battery pack will hold 195 cells in series and 9 cells in parallel to provide the energy required for the motor. All battery packs will be connected together in a parallel configuration so that working packs can still provide energy in the event of a single pack failure.

C. Charging

There are 3 types of vehicle chargers. Level 1 and Level 2 are used in residential applications. 110/120 volts and 12 to 16 amps of continuous power is used for level 1, and 208/240 volts and 16 to 40 amps of continuous power for level 2. These chargers are capable of charging high-energy-density electric vehicles, however, charging takes a significant amount of time. The third type is called DC fast electric vehicle charger. This charger is marketed as a fast charger for electric cars. This charger uses between 200 to 600 volts and 100+ amps. This new charging technology significantly improves charging time for current electric vehicles. According to an article from Electrek[17], a Tesla car with 100 kWh (134.05 hphr) takes 20-40 hours using level 1 AC (120V outlet at home), 8-12 hours using level 2, and only 15-25 minutes using DC fast charger.

Blitzen is a commercial aircraft profiting on rapid cycle times, therefore, the time spent on charging will be a crucial factor. Table 15, shows the time required to charge the battery from 0% to 100% using chargers of various power

Table 15 Charging Duration

	Charger (kW)					
	100	120	150	200	270	350
Battery Capacity (kWh)	**Duration (hr:min:sec)**					
10	0:06:40	0:05:33	0:04:27	0:03:20	0:02:28	0:01:54
100	1:06:40	0:55:33	0:44:27	0:33:20	0:24:41	0:19:03
200	2:13:20	1:51:07	1:28:53	1:06:40	0:49:23	0:38:06
287	3:11:20	2:39:27	2:07:33	1:35:40	1:10:52	0:54:40

capabilities. The most powerful charger with 350kW, requires 54 minutes 40 seconds. This duration considers a battery when it is fully discharged, therefore, the actual charging time will be shorter than the time listed on the table since the aircraft will rarely discharge completely.

D. Battery Life Expectancy

Every battery has a varying life expectancy depending on its use and environment. One charge cycle is defined as one full discharge and a full recharge. A battery degrades slightly after every charge cycle. Additionally, even without a completing a charge cycle, time and temperature reduce the battery life expectancy due to an increase in the internal resistance, loss of electrolytes, and crystallization of electrodes. Currently, typical batteries last 18 months to 3 years [18], and they start deteriorating rapidly after this period.

Due to high battery costs, battery life expectancy is important. This is especially true for an eVTOL air taxi expected to undergo many charging cycles quickly. This directly implies the battery life expectancy will be shorter than expected and will require more frequent battery replacement. Current battery replacement cost for electric vehicles ranges from $5000 to $7000 for each module and replacing the entire battery pack ranges from $30,000 to $42,000.

IX. Airframe Structural Design

A. Airframe Structure

Blitzen's structural design prioritizes safety, comfort, and accessibility for all passengers. The cabin is spacious for easy boarding and storage of personal belongings or accommodating medical devices. The structure also allocates sufficient space for the helicopter's electrical system. One section of the fuselage is dedicated entirely to the large and heavy battery packs. Other fuselage sections include the cockpit, cabin, and luggage storage.

Blitzen's structure follows a semi-monocoque design. This design includes bulkheads, longerons, and stringers covered by an external skin. The combination of internal structures and an external skin allows the rotorcraft to retain its shape under load. All of these components diffuse loads throughout the airframe to create a strong structure that can continue safe flight in the event of a single failure. These components are installed throughout the three main structural segments of the helicopter: fuselage, tail, and cowling.

B. Fuselage

The fuselage consists of ten primary I-beam bulkheads that are connected with stringers and longerons (Figure 34). These stringers and longerons help to prevent fuselage bending in flight by handling tension and compression stresses. Two keel beams are located under the floor of the helicopter to support bulkheads. The upper deck consists of bulkheads and two keel beams for support. The two wingspan-length wing spars fasten to the fuselage at concurrent bulkheads. These two spars, located at the wing's 20 and 50 percent chord marks, connect to the fifth and sixth fuselage bulkheads from the nose of the helicopter, respectively. The wing spars pass through the fuselage structure because they are single uncut beams. The wing skin smoothly transitions to the fuselage exterior skin using a wing-to-body fairing.

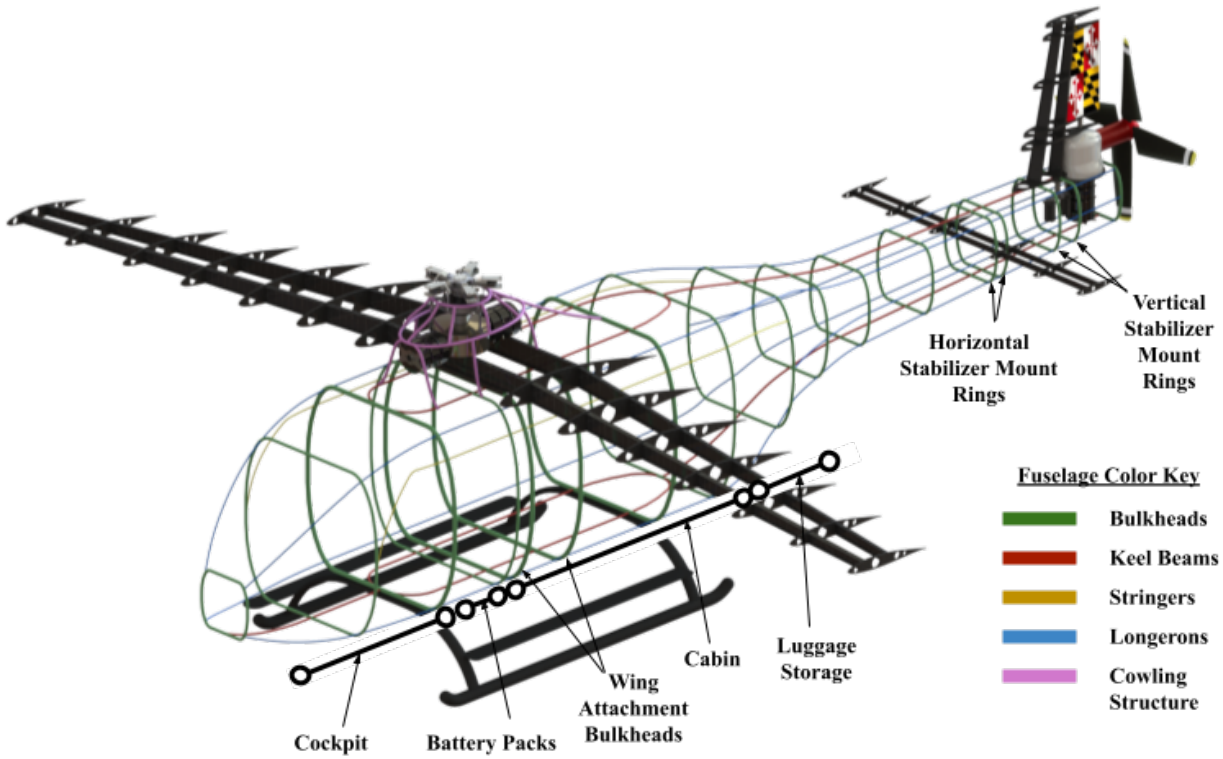

Fig. 34 Fuselage Airframe Structure

C. Tail and Empennage

The empennage stems from the fuselage and has a horizontal and vertical stabilizer constructed with similar materials selected for manufacturing ease and strength. The empennage sustains loads among multiple axes due to the swiveling rotorprop, so a rigid design is needed. The empennage therefore consists of 7 bulkheads connected with longerons for support, totalling 17 bulkheads in the airframe. The motors for the swivel mechanism are held in between the mount ring bulkheads for the vertical stabilizer. The rotorprop motors are fastened the aft-most end of the tail behind the vertical stabilizer bulkheads and below the swivel mechanism.

The horizontal and vertical stabilizer spars are mounted to bulkheads that are held by cantilevered beams. The stabilizer ribs are connected to the spars at the 20% and 50% chord locations. The horizontal stabilizer is forward of the vertical stabilizer to make space for the swiveling rotorprop mount at the end of the tail. The horizontal stabilizer has a similar structure to the wing shown previously, with a carbon fiber rib and spar structure without taper. The stabilizer features a two unified spars passing through both fin sides and the empennage. Bulkheads attach the stabilizers to the main structure and help dissipate any loads that the fins experience. The vertical stabilizer's structure supports the rudder and holds the required airfoil shape. The structure consists of a rib and spar design similar to the horizontal stabilizer.

D. Cowling

The cowling structure consists of stringers and three bulkheads. The cowling section provides shape-holding for the exterior skin. The main rotor gearbox, wing spars, and main motors attach to bulkheads on the floor of the cowling and are enclosed by the cowling skin surface. The cowling and the components it encases can be seen embedded in the structure in Figure 34.

E. Landing Gear

Fixed skids were chosen for the landing gear due to their simplicity and weight. The cross tubes are elliptical to be more aerodynamic. Skid landing gear also requires little maintenance. Landing gear with wheels were considered but not chosen as they add additional weight and complexity to the helicopter structure and increase maintenance requirements. A step is attached to the landing gear to aid able-bodied passengers and the pilot with ingress and egress.

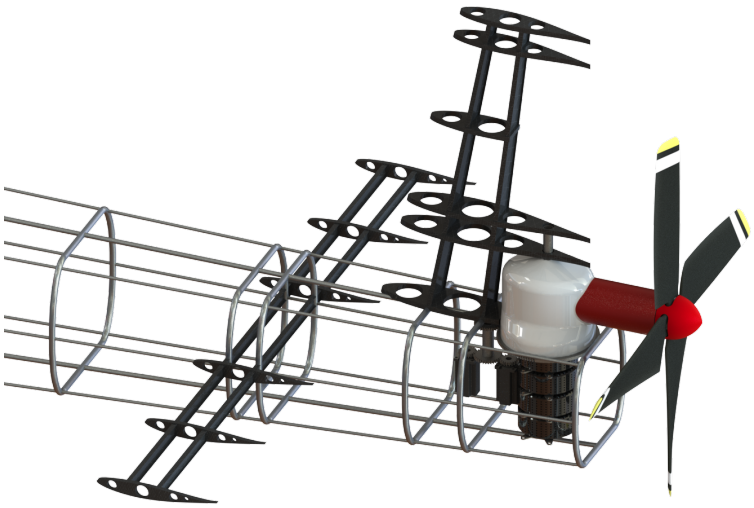

Fig. 35 Empennage Structure

Finite element analysis (FEA) was conducted on the landing gear to ensure that it can sustain the impact load of the helicopter while landing.

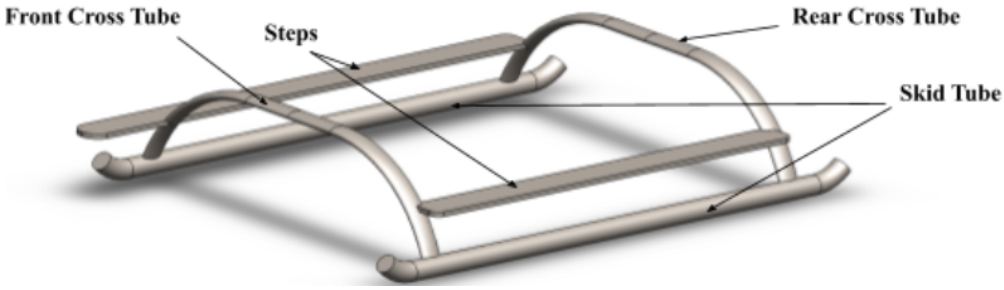

Fig. 36 Landing Gear

The FEA demonstrated that the steel (AISI 4340) landing gear can sufficiently withstand the weight of the helicopter while landing, and stays well under its yield stress. The added step on the landing gear is not included in this analysis as it will not be load-bearing. The assumptions made during this study include: the impact force is equivalent to a load factor of 2.5g, forces are applied by the ground at critical nodes, and the coefficient of friction between the skids and ground is $\mu_f = 0.4$ [19]. The stress and deformation analyses are shown in Figures 37 and 38. The impact load and friction between ground and landing gear were applied at the joints between the cross tubes and the skid tubes. The stress diffuses throughout the cross tubes. The landing gear attaches to the fuselage at set fixtures to keep those points constrained in all principal direction [19]. The total mass of the helicopter is 2648.5 kg (5838.6 lb), and the load factor is applied to this mass. This is seen in Equation 14 to get the total force in the z-direction that the landing gear has to endure.

$$F_z = 2649kg \times 2.5g \times \left(9.81\left(\frac{m}{s^2}\right)/4\right) = 16241.68N\ (3651.27lbf) \tag{14}$$

The frictional force between the ground and landing gear is in the y-direction at the critical nodes and can be calculated by multiplying the weight force by the coefficient of friction.

$$F_y = 16241.68N \times (0.4) = 6496.672N\ (1460.51lbf) \tag{15}$$

Because of the semi-monocoque structure, any high impact can be diffused into the fuselage airframe where the cross tubes connect with the main structure. The safety factor for this incident is 2.7, further reinforcing that the skid landing gear is able to withstand the load of the helicopter with a simple, light-weight, and cost-effective design.

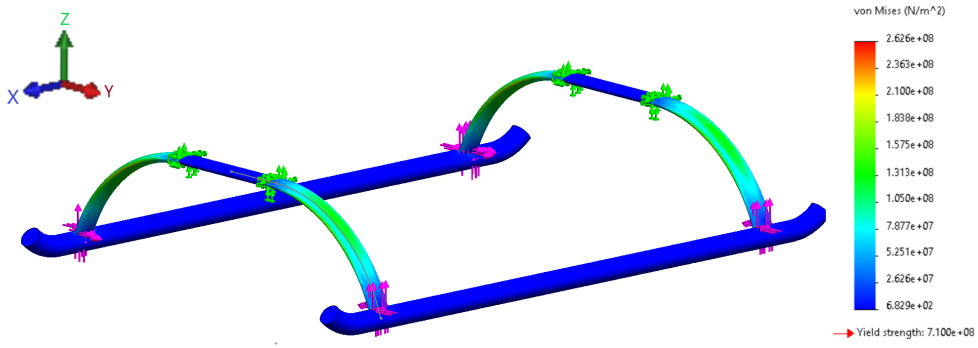

Fig. 37 Stress on Landing Gear

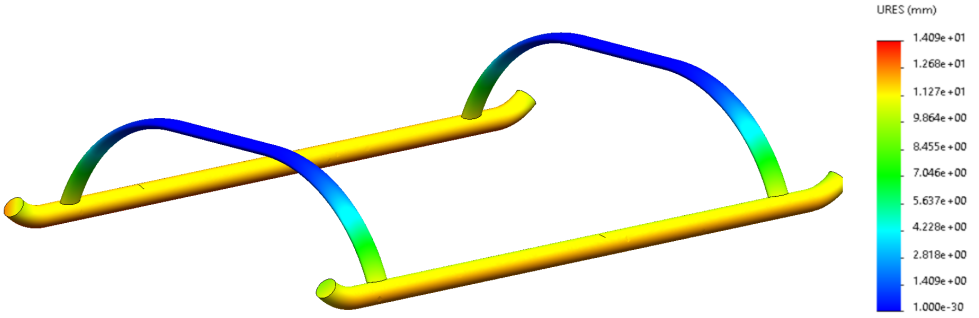

Fig. 38 Deformation of Landing Gear

F. Load Paths

While the helicopter is on the ground, the load path starts at the bulkheads and terminates at the landing gear. The loads travel through longerons and keel beams along this path.

While the vehicle is in flight, the weight of the helicopter, its components, the thrust from the main rotor, and the anti-torque from the tail rotor cause concentrated stresses on parts of the structure the structure. These loads are diffused into the rest of the structure via the bulkheads, deck beams, and longerons. The amount of these parts included in the structure was chosen to properly diffuse the loads while not adding too much weight to the helicopter.

G. Material Selection

The skin of the entire helicopter is made of fiberglass/epoxy. This material is very lightweight, strong, and has a high resistance against corrosion and heat. Kevlar/epoxy was also considered because of its ability to protect against pebbles and other debris that may impact the helicopter due to downwash from the main rotor [7], but it was not chosen since it is very sensitive to ultraviolet radiation. Because of the photo degradation on the fibers, the material will become more brittle, more susceptible to cracking on the surface, and likely to change color [20]. Fiberglass/epoxy has a high resistance to ultraviolet radiation and does not exhibit degradation.

Aluminum is commonly used among helicopter structures because it is lightweight, has a good strength-to-weight ratio, and is relatively low-cost. In addition, using an aluminum-lithium alloy will lower the density of the material while also improving the elastic modulus and resistance to fatigue cracking. For these reasons, the bulkheads, longerons, and stringers of the entire helicopter are made of aluminum-lithium alloy. The flooring of the helicopter is made of 6061 aluminum sheets because it's lightweight and very durable, whereas steel would have been much heavier. The windows are made of polycarbonate because of its high resistance to cracking and breaking. It is lightweight and provides insulation while also having a high capacity for heat resistance and protection against UV rays. Moreover, polycarbonate can be heat-formed to the complex windshield geometry without decreasing optical clarity.

X. Avionics

Blitzen is a commercial air taxi and thus should be ready to fly during any time it is needed. Blitzen needs certain avionic and sensor equipment to allow it to fly in visual flight rules (VFR) and instrument flight rules (IFR) conditions, as well as specific equipment to allow Blitzen to fly all types of airspace. Blitzen utilizes a "glass-cockpit" avionics suite, featuring a large LCD screen with digital flight instruments rather than the typical analog dials and gauges. Analog dials and gauges, and their redundant additions, would take up an incredible amount of space in the cockpit, potentially reducing the pilots field of vision.

A. Thales FlytX Avionics Suite

The Thales FlytX avionics and sensor suite for helicopters was chosen as the primary avionics display because it offers a wide array of features for both IFR and VFR flight while having compact form factor [21]. The Thales FlytX offers various flight display configurations which can be tailored for different helicopters depending on the intended mission or area of operation. The FlytX with a Integrated Display Unit or iDU, (Figure. 41), allows Blitzen to display primary flight instruments, powerplant monitoring panes, navigation moving maps, and radio equipment on the same screen in a compact manner. This flight display also includes synthetic vision systems (SVS) allowing for an even greater understanding of the surrounding area during instrument meteorological conditions (IMC) and night flight. FlytX also includes a digital map, basic flight management systems, flight warning systems, centralized maintenance system, standby instruments, as part of its base package. In terms of probes and sensors, FlytX offers an air data units (ADU) and heated pressure probes as well as VHF omnidirectional range and instrument landing system (VOR/ILS) functionality as part of its base package for a single pilot interface. The FlytX suite also offers three and four axis autopilot and flight and voice data recorders as optional upgrades.

Fig. 39 Cockpit Layout of the Thales FlytX Avionics Suite

B. External Lighting

Blitzen's mission expects operation during most weather and daylight conditions. Therefore, the vehicle includes external navigation lights, similar to those seen on a traditional aircraft. Blitzen has a red light on the tip of its left wing, a green light on the tip of its right wing, and a white light on the end of its tail. The vehicle also features na anti-collision light located on the fuselage aft of the rear landing gear cross tube. Landing lights will be located under the cockpit area facing forward, to illuminate the landing location and improve vehicle visibility to people on the ground [22]. Dual electrical systems for all external lights are installed for redundancy.

XI. Flight Controls

Blitzen's control scheme was designed to mimic the control scheme of other helicopters. Blitzen features a conventional cyclic, collective, foot pedals, and throttle, in their standard position and their standard uses. This similar control scheme was made to significantly decrease the amount of training required by any pilot familiar with different helicopters. Blitzen will use traditional helicopter controls in a fly by wire configuration, where there will be no mechanical linkages to control surfaces and actuators. Instead every control will be attached to their respective surfaces by a wire. Because of the complexity of the swiveling tail system and the use of a rudder, some deviations from the standard helicopter control system are needed.

A. Cyclic & Collective

In an effort to keep standardized controls for all flight modes, the cyclic, collective, and throttle will act in the same manner as in a traditional helicopter. The signals from the cyclic and collective potentiometers are sent to a control

computer which will compare the signals using majority voting. Four signals are input to the computer and compared. The computer will output the signal obtained from a majority of the wires to the control surfaces and actuators. Majority voting allows for redundancy in flight control signals input by the pilot to the surfaces while also eliminating any false signals given to the flight computer from outside sources.

B. Foot Pedals

Yaw control is provided by two differing methods in hover and cruise. In an effort to keep the control system as simple as possible, the tail control inputs for both the tail rotor and rudder will originate from the foot pedals. When Blitzen is in "hover mode" the inputs from the foot pedals will go to the tail rotor. When Blizten switches to "cruise mode" the inputs from the foot pedals will go to the rudder. Pilot inputs on the foot pedals will be read by a potentiometer. Signals sent through four wires, for redundancy, to a flight computer using majority voting to generate an output. The flight computer will determine whether the aircraft is in "hover mode" or "cruise mode" via flight velocity and send the signal from the foot pedals to their corresponding control surfaces.

C. Pilot-Cockpit Interaction

Due to the nature of a fly-by-wire configuration there will be a distinct lack of feedback given to the pilot from control actuators and surfaces. Blitzen utilizes springs on the cyclic control stick to simulate force feedback. The springs also return the stick to its neutral position if no input is given by the pilot.

The glass cockpit avionics and windows are positioned to allow the pilot to exceed a standard ± 15° vertical field of view from the horizontal plane [7]. In addition, windows on the floor aid in vertical takeoff and landing. The pilot also has over 180° of horizontal field of view through windows placed around the cockpit.

XII. Cabin Configurations and Features for Passengers with Disabilities

A. Cabin Seating Configurations

Blitzen has two primary configurations: four-seats (Figure 40a) and two-seats (Figure 40b). Both configurations consist of two rows with seats facing each other. Two other configurations were considered and ultimately not chosen for the vehicle: all seats facing the front of the aircraft shown in Figure 40c and seats facing into the center of the cabin in a sideways configuration shown in Figure 40d. The seating configurations chosen maximizes space efficiency in addition to providing large amounts of leg room and adding a conversational atmosphere compared to the other two configurations. Two seats get removed, one from each row on the other side from one another, to transition from

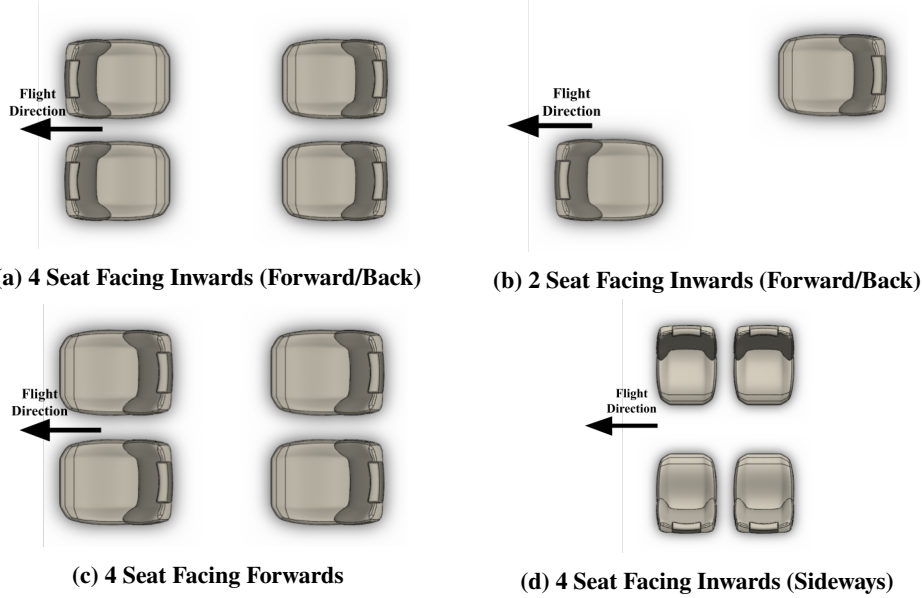

(a) 4 Seat Facing Inwards (Forward/Back)

(b) 2 Seat Facing Inwards (Forward/Back)

(c) 4 Seat Facing Forwards

(d) 4 Seat Facing Inwards (Sideways)

Fig. 40 Configurations

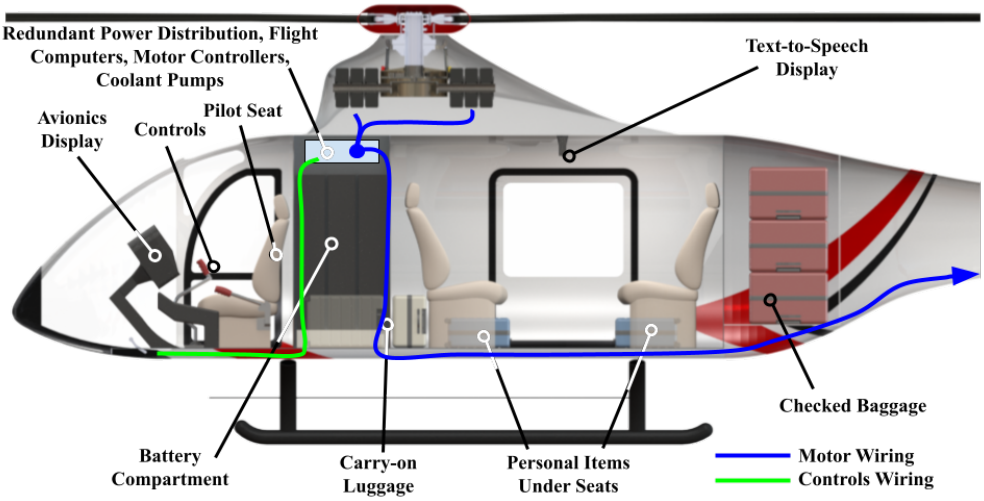

Fig. 41 Side View Cutaway

the four-seat cabin to the two-seat cabin. This was done to aid ingress and egress for people needing more complex disability accommodations. For example, passengers in wheelchairs may position themselves directly next to an aircraft seat before transferring themselves to the seat and getting assistance to put their wheelchair in the luggage compartment. Although the two cabin seating configurations are presented, any seating combination with the four seats included or removed is feasible. Personal items are to be stowed away under the passenger seats. Carry on luggage is stored behind the first row of seats between the battery compartments and passengers as shown in Figure 41. The carry on luggage will be held in place by a net system. The carry-on luggage compartment also has space to accommodate medical equipment that needs to be carried with the passenger at all times.

B. Luggage Compartment

Blitzen features a luggage compartment behind the main passenger cabin. Four bags, up to standard-sized airline baggage dimensioned in Figure 42, can fit within the baggage compartment. The compartment can accomodate additional medical equipment such as folding wheelchairs and crutches when the aircraft is transporting two disabled passengers. The luggage compartment is accessible via a large latching door on the exterior of the aircraft.

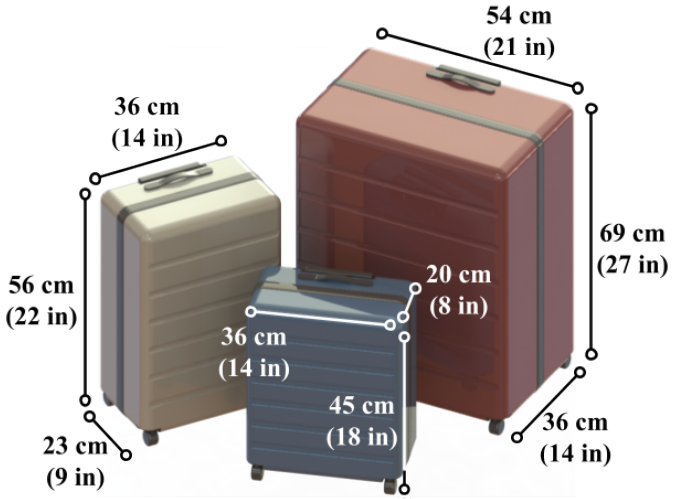

Fig. 42 Dimensions of Carry-on Item, Personal Item, and Checked Baggage

C. Features

According to Edwards and Price in a NASA eVTOL passenger acceptance study, "passengers' acceptance of safety is the most important concern" identified for the successful widespread use of eVTOL vehicles [23]. Blitzen's cabin was configured withe features to improve perception of safety for all passengers. Six major features that improve customer

perception of safety are present in the cabin. These features improve air-taxi service accessibility for customers with disabilities.

- Handles are present on walls and ceilings for passengers to use during boarding and periods of discomfort caused by turbulence.
- Headsets with microphones are given to each passenger to communicate with the pilot. Non-verbal or deaf passengers are also provided with a keyboard with text-to-speech capabilities attached to the same communication line as the headsets.
- A speech-to-text display is mounted to the ceiling in the center of the cabin in view of all passengers. The display is connected to the pilot's microphone and is used for communication from pilot to the passengers. This augments pilot announcements over headsets with a visible representation.
- Dimmable high-intensity lighting is present in the cabin if needed by passengers with limited vision. The cabin can be dimmed when passengers without vision disabilities are transported or during nighttime.
- Emergency buttons and respective high-visibility decals are located on every seat in the cabin. Passengers can use these buttons to alert the pilot in the event of an emergency in the cabin.
- Passenger air vents are installed on the cabin's walls. These can be used for cabin air circulation and cooling in forward flight in addition to providing air to airsick passengers. This is a simpler and lighter solution to cabin climate control over a dedicated air conditioning system installed in the aircraft.

XIII. Concept of Operations (CONOPS)

A. Vehicle Footprint

Blitzen's operation in an urban environment relies on its small footprint. The RFP requests a maximum footprint of of 15.24 m (50 ft) by 15.24 m (50 ft) with rotors turning. The Blitzen exceeds this requirement, as shown in Figure 43.

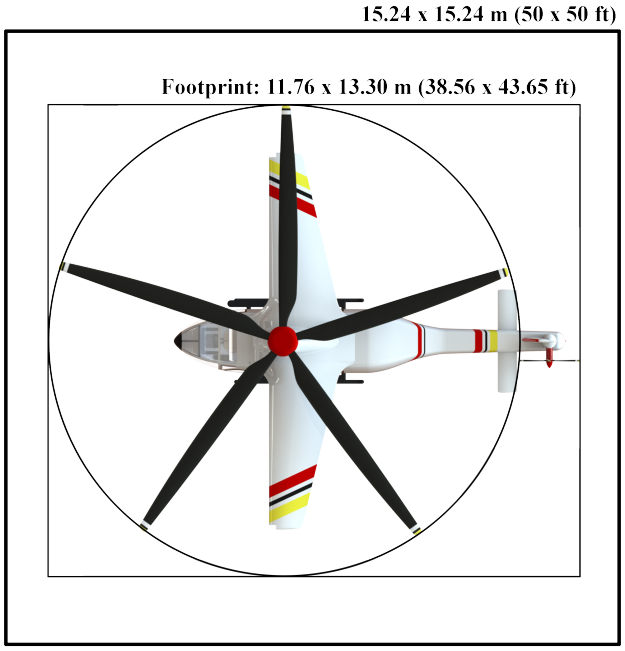

Fig. 43 Blitzen Footprint with All Rotors Turning

B. Pre-Flight Operations

Accommodating passengers with disabilities does not stop at including supportive features within the vehicle. It also involves making them feel comfortable with the whole process of riding an air taxi. Preflight processes must be very accessible for passengers for them to feel secure in their choice of transportation. Blitzen's operators provide clear information about the flight to passengers before traveling. When booking, passengers can inform the operator of their disabilities so there is sufficient time to prepare their accommodations before the flight. The pilot and ground crew have extra training to assist passengers with various disabilities. Passengers have the option to go on a familiarization visit to the airport prior to their day of travel to alleviate stress and anxiety about their trip. Even if passengers do not need all of these accommodations, the website is still very informative of the whole process of riding an urban air taxi, as this is a relatively new concept. All forms of communication clearly mention that the Blitzen is a very accommodating travel option, and anyone is welcome.

C. Ingress and Egress

Blitzen's landing gear has a step, as seen in figure (Fig. 36), to make it easier for the pilot and passengers to enter and exit the vehicle, which is 0.55 m (21.5 ft) off of the ground. Passengers who use a wheelchair or are otherwise unable to use the step to board Blitzen will be provided a wheelchair lift that is stored on site. Two circular mounts in the floor of the cabin hold the wheelchair lift while in use. Passengers who use wheelchairs will be assisted by the ground crew onto the lift (Figure 44). A motorized torque tool connects to the top of the wheelchair lift to raise the lift platform. Passengers will then enter the cabin and orient their wheelchair to align next to the passenger's seat. Passengers will then sit themselves in their seat. Having the passengers seat themselves as they would typically do in any other vehicle increases passenger comfort and does not infringe on a passenger's personal space.

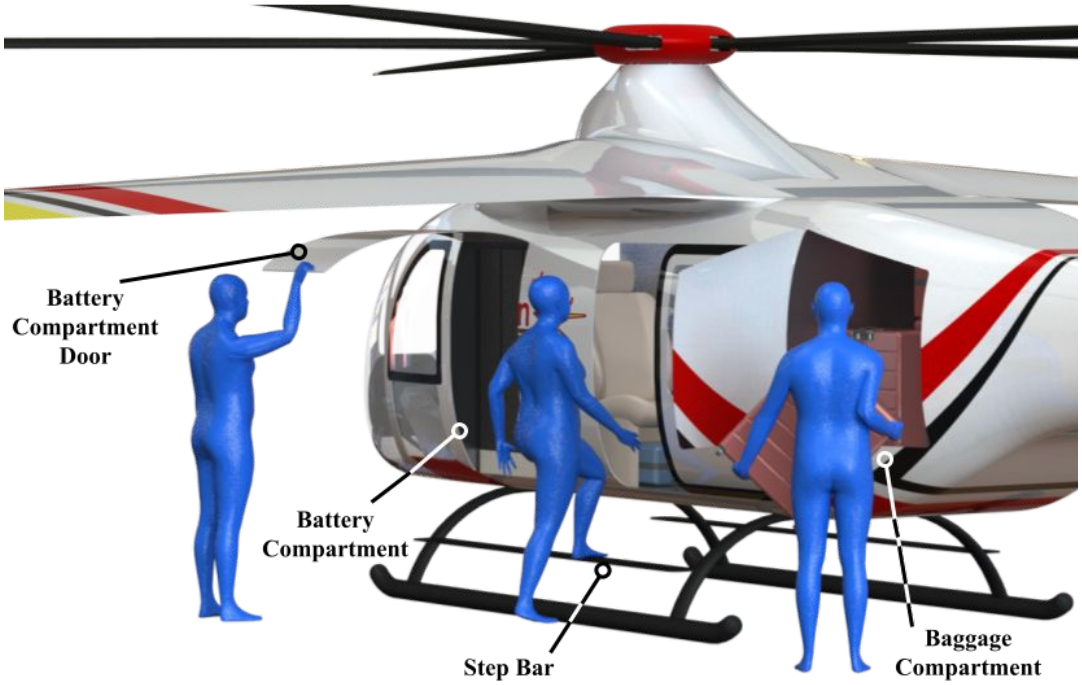

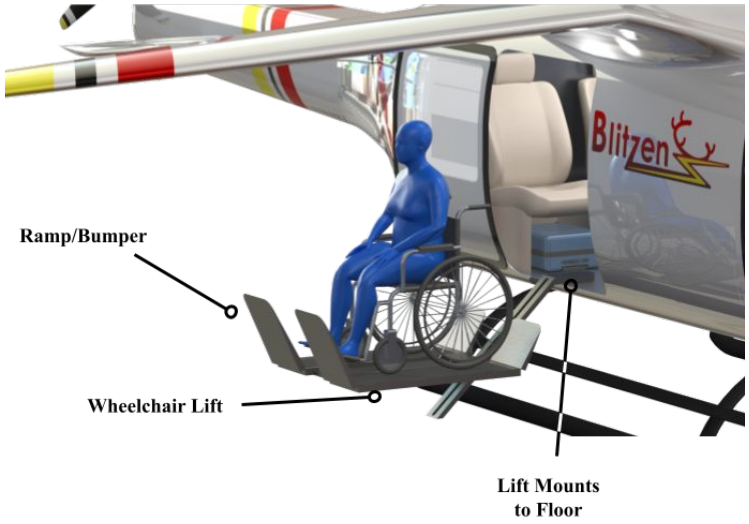

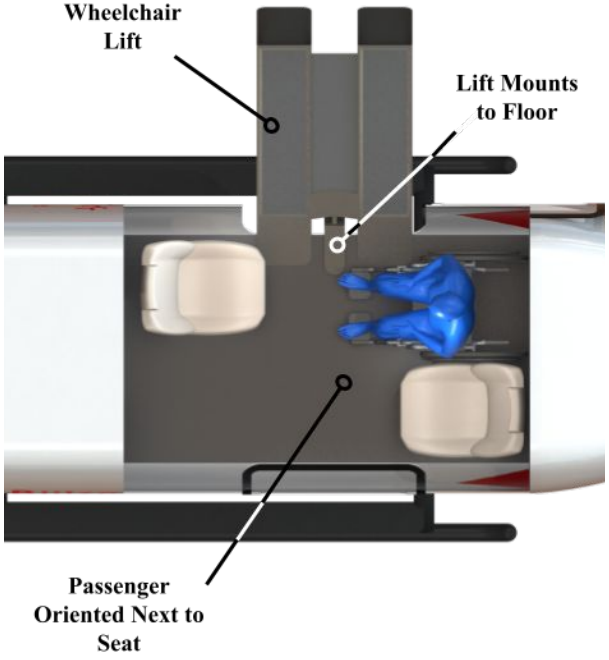

(1) Preflight ground crew opens the battery compartment to either remove depleted batteries to be charged on site and replaces with charged batteries or charges them in the vehicle.

(2) Passengers who use wheelchairs will be moved onto the lift with front ramps. The ramps will then rotate up to prevent passengers from rolling off.

(3) Lift reaches vehicle floor and rear ramps are laid down. Passenger is moved off of ramp and oriented with their seat.

(4) Wheelchair bound passenger moves on their own to the seat next to the wheelchair.

(5) Ground crew folds the passenger's wheelchair and stores it in the baggage compartment.

Fig. 44 Blitzen Before Flight Procedures

Each passenger is allowed one personal item, one carry-on item, and one piece of checked baggage. The maximum allowable weights and dimensions of the baggage is given in Figure 42; it is important to note that the checked bag has a maximum total linear dimension of 158 cm (62 in), but the figure depicts the most common size for a checked suitcase.

D. Procedure Between Flights

Batteries can be charged in the vehicle or replaced depending on required mission turnaround time. Both battery compartments are accessible using side doors (Figure 44). Batteries are located behind the pilot and are separated into two compartments. Both compartments are accessible through side doors.

When changing from the four-seat configuration (Figure 40a) to the two-seat configuration (Figure 40b), seats will be removed and stored on-site.

E. Transition Between Hover and Cruise

Transition between hover and cruise follows a linear task order. When the vehicle is in hover, the swiveling rotorprop will be in anti-torque mode. Initial acceleration is achieved by pitching the rotorcraft forward. Once sufficient velocity is reached for the the vertical stabilizer with deflected rudder to counter main rotor torque, the rotorprop transitions to cruise mode and the vehicle returns to level pitch. Using the commands received from the flight computer, the rotorprop automatically decreases power, swivels 90 degrees and locks into cruise position, and increases power to act as a pusher propeller. The pilot also has a manual swivel override to immediately transition the mechanism to either state. Both swivel system configurations are illustrated in Figure 45.

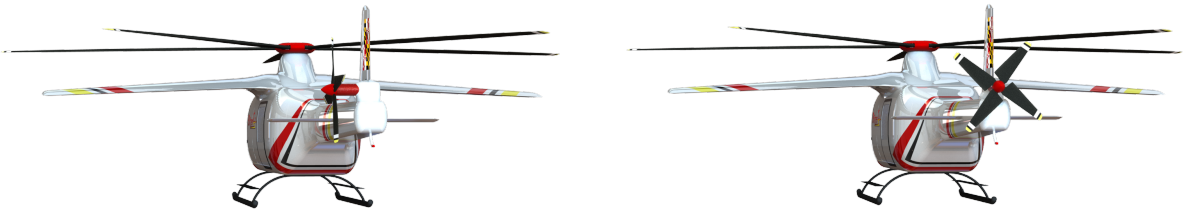

(a) Hover Configuration **(b) Cruise Configuration**

Fig. 45 Swiveling Rotorprop Configurations

F. Center of Gravity Envelope

The vehicle's center of gravity was designed to be as close as possible to the main rotor shaft and wing quarter chord to minimize additional control inputs in flight. In addition, the center of gravity changes minimally with various numbers of passengers and baggage since the cabin moment arm is minimal. The vehicle center of gravity is illustrated in two axes in Figure 46.

The physical dimensions of the landing gear are determined after analysis of the center of gravity to ensure stability. For roll stability, the tip over angle is less than 60°. For pitch stability, the pitch angle is greater than 30°. The rear end of the landing gear is also be far enough aft to avoid a tail strike with an inclination of 12° [7]. As shown in the figures below, Blitzen exceeds these guidelines. Additionally, Blitzen features a tailskid to limit damage in the event of a tailstrike.

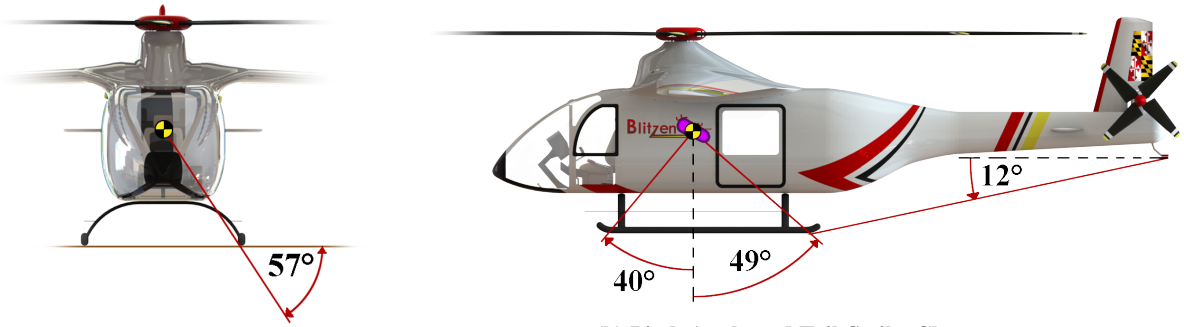

(a) Tip Over Angle **(b) Pitch Angle and Tail-Strike Clearance**

Fig. 46 Center of Gravity and Static Stability Angles

XIV. Aircraft Acoustics

A. Computation of Acoustics

The Blitzen's acoustics were calculated using a code developed in-house that uses Robert J. Pegg's method as outlined in [24]. The method computes the rotational noise of the main and tail rotor, the compressibility induced drag noise, the thickness noise, and the blade vortex interaction noise separately over a range of harmonics. The magnitude of each type of noise produced at each harmonic are combined to get the amplitude of the noise at a specific point in space. Pegg's method assumes the aircraft has a single main rotor and side-mounted tail rotor, so the blade vortex interaction noise will have different profile than calculated; however, the primary goal of this analysis is to gain of general view of the vehicles acoustic profile composed of broadband, thickness, and compressibility induced drag noise.

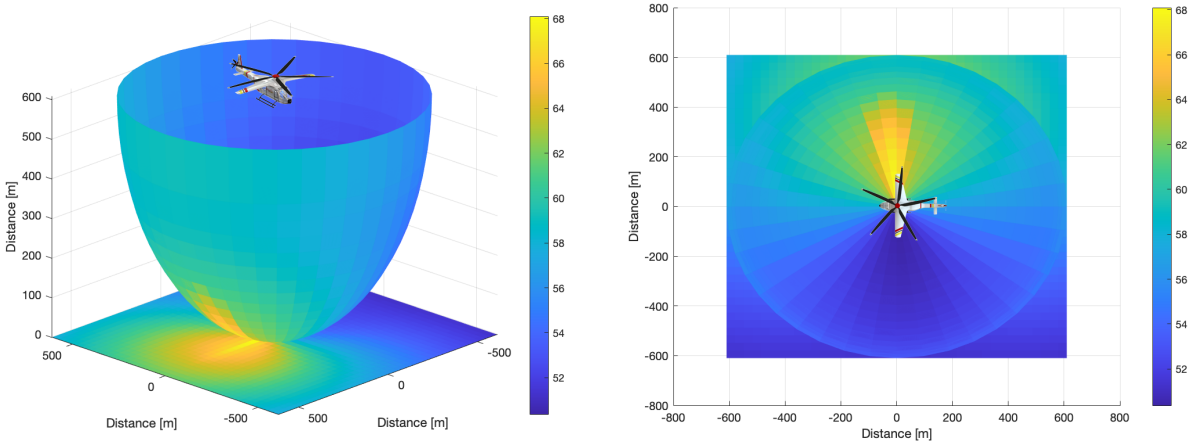

(a) Isometric View

(b) Top View

Fig. 47 Blitzen Acoustic Field in Cruising Flight

B. Acoustic Analysis

Figure 47 depicts the acoustic profile of Blitzen while in cruising flight. The altitude chosen for this analysis was chosen as the cruise altitude from the RFP (609.6 m (200 ft) AGL). The overall sound pressure level was calculated along the surface of the ground and a hemisphere of radius 609.6 m. The highest noise level was 68 dB under the advancing blades of the main rotor. 68 db is comparable to an average conversation that is on the louder side. This low-profile sound will allow the Blitzen to become a part of daily life without interrupting it and disturbing the areas the vehicle flies over.

XV. Safety

A. US Code of Federal Regulations Compliance (14 CFR 29)

The RFP states that "the design shall conform to the applicable requirements of 14 CFR 29 – US Code of Federal Regulations (CFR) Title 14 (Aeronautics and Space) Airworthiness Standard". Table 16 represents the compliance that Blitzen made to comply with the US regulation as a transport category rotorcraft.

Table 16 14 CFR 29 Compliance

Title	Regulations	Compliance
§ 29.771 Pilot compartment.	Each pilot compartment must be arranged to give the pilots a sufficiently extensive, clear, and undistorted view for safe operation.	The rotor head design ensures low vibrations; instrument panel is mounted on shock absorbers.

§ 29.771 Pilot compartment.	(c) The vibration and noise characteristics of cockpit appurtenances may not interfere with safe operation; Each pilot compartment must be free of glare and reflection that could interfere with the pilot's view.	Cockpit and shield contoured to ensure freedom from glare and reflection. Refer to Figure 41
§ 29.775 Windshields and windows	Windshields and windows must be made of material that will not break into dangerous fragments.	Poly-carbonate will be used. Reference in Section IX
§ 29.777 Cockpit controls	(a) Located to provide convenient operation and to prevent confusion and inadvertent operation; (b) Located and arranged with respect to the pilotś seats so that there is full and unrestricted movement of each control without interference from the cockpit structure or the pilot's clothing when pilots from 52 to 60 in height are seated	Reference in Section X
§ 29.779 Motion and effect of cockpit controls	(a) Flight controls, including the collective pitch control, must operate with a sense of motion which corresponds to the effect on the rotorcraft. (b) Twist-grip engine power controls must be designed so that, for left hand operation... (c) Normal landing gear controls must operate downward to extend the landing gear.	Reference in Section X, and Section IX
§ 29.783 Doors	(a) Each closed cabin must have at least one adequate and easily accessible external door. (b) Each external door must be located, and appropriate operating procedures must be established... (c) There must be means for locking crew and external passenger doors and for preventing their opening in flight inadvertently or as a result of mechanical failure.	Reference in Section IX
§ 29.785 Seats, berths, litters, safety belts, and harnesses	(f) Each seat and its supporting structure must be designed for an occupant weight of at least 170 pounds, considering the maximum load factors, inertial forces, and reactions between the occupant, seat, and safety belt or harness corresponding with the applicable flight and ground-load conditions, including the emergency landing conditions of § 29.561(b).	Safety equipment will be installed in the aircraft with accordance to the guideline
§ 29.787 Cargo and baggage compartments	(a) Each cargo and baggage compartment must be designed for its placarded maximum weight of contents and for the critical load... (b) There must be means to prevent the contents of any compartment from becoming a hazard by shifting under the loads specified in paragraph (a) of this section. (d) If cargo compartment lamps are installed, each lamp must be installed so as to prevent contact between lamp bulb and cargo.	There will be nets and walls to secure luggage.
§ 29.803 Emergency evacuation	(a) Each crew and passenger area must have means for rapid evacuation in a crash landing, with the landing gear	Reference in Section XIII

§ 29.805 Flight crew emergency exits	(a) For rotorcraft with passenger emergency exits that are not convenient to the flight crew, there must be flight crew emergency exits, on both sides of the rotorcraft or as a top hatch, in the flight crew area.	Reference in Section XIII
§ 29.807 Passenger emergency exits	(4) Type IV. This type must have a rectangular opening of not less than 19 inches wide by 26 inches high, with corner radii not greater than one-third the width of the exit, in the side of the fuselage with a step-up inside the rotorcraft of not more than 29 inches. Openings with dimensions larger than those specified in this section may be used, regardless of shape, if the base of the opening has a flat surface of not less than the specified width.	Reference in Section XIII
§ 29.809 Emergency exit arrangement	(a) Each emergency exit must consist of a movable door or hatch in the external walls of the fuselage and must provide an unobstructed opening to the outside. (b) Each emergency exit must be openable from the inside and from the outside. (c) The means of opening each emergency exit must be simple and obvious and may not require exceptional effort.	Reference in Section XIII
§ 29.812 Emergency exit access	(c) There must be access from each aisle to each Type III and Type IV exit	Reference in Section XIII

B. Battery Failure Analysis

The RFP requires safe flight following any single failure of the electrical power distribution system, including the batteries. Multiple solutions to this were considered. The most common solution is to distribute energy storage amongst multiple separate battery packs, as it minimizes energy losses following a single failure. The second solution considered was choosing an alternate landing site in the event of a failure. When asked about landing in the event of a power distribution failure, Bell responded that "the alternative landing site may be selected by the team between the origin and the destination for a safe flight following any single point failure." The team selected various locations for analyzing safe landing alternatives in the event of a single failure.

1. Energy Remaining and Allowable Flight Distance

Equation 16 is used to calculate energy remaining after a battery pack failure at a certain point in the flight. Remaining energy is also dependent on the number of battery packs, which can be used to determine the desirable number of packs to include. Figure 48 shows the energy remaining versus distance already traveled when a battery pack failure occurs. The different colored curves correspond to vehicles with different numbers of battery packs. The dashed curve illustrates energy remaining if no failure occurs.

$$Energy_{remaining} = (Energy_{total} - Energy_{consumed}) * \frac{(N_{batteries} - 1)}{(N_{batteries})} \tag{16}$$

$$Distance = \frac{Energy_{remaining}}{Energy_{required}} * 100miles \tag{17}$$

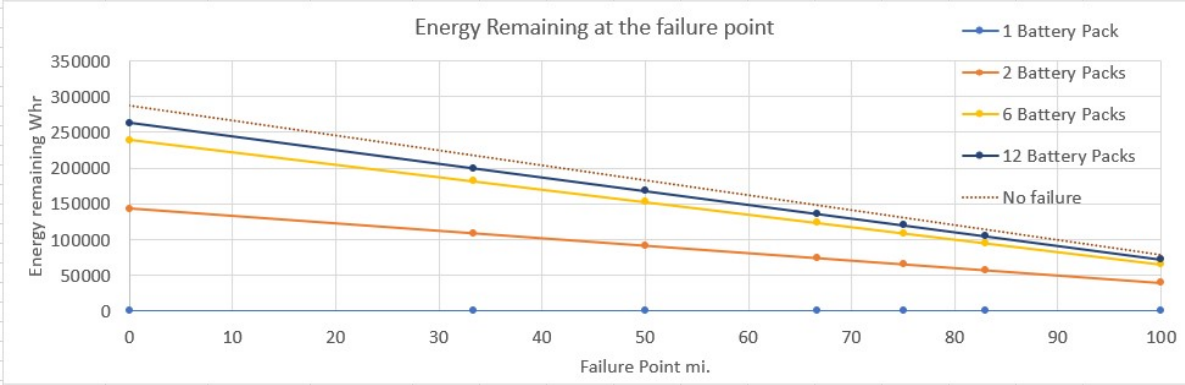

Fig. 48 Energy Remaining after a Single Battery Pack Failure

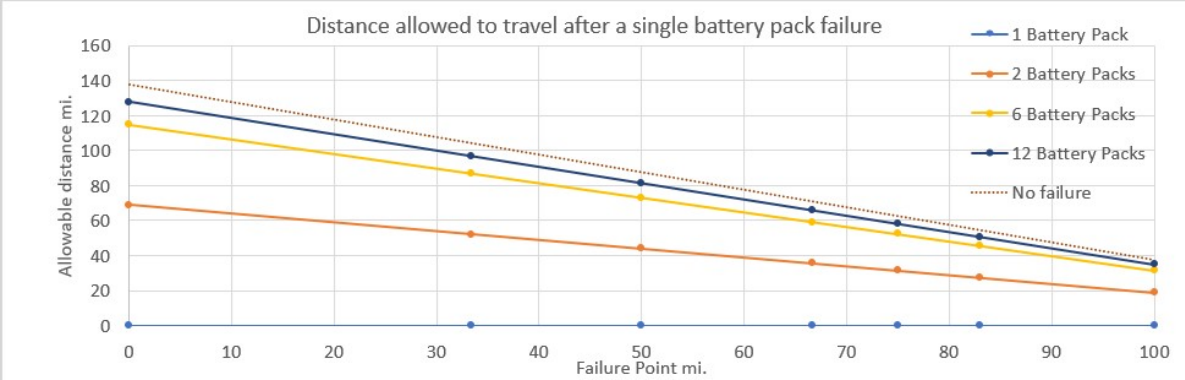

Fig. 49 Distance Remaining after a Single Battery Pack Failure

Equation 17 is used to calculate the distance that the aircraft can travel after a battery pack failure, and Figure 49 shows the remaining range after a single pack failure for vehicles with different numbers of battery packs.

2. Energy Remaining in Various Alternate Landing Zones

After plotting the remaining range from the failure point, the energy remaining versus failure distance from the starting position was calculated. The graphs in Figure 50 show energy remaining after traveling to alternate landing sites from the failure point. For these calculations, it was assumed that the alternate landing sites were along the flight path; in other words, the takeoff site, landing site, and Blitzen's current position were all colinear. The titles of the graphs in Figure 50 describe the distance along the flight path of the landing site from the takeoff site. Alternate landing sites at 50, 66, and 75 miles from the takeoff site were selected because once the aircraft passes the half-way point of its mission, there is not enough energy reserves in event of a single pack failure to guarantee safe flight back to the takeoff site or destination.

According to Figure 50a, landing at the 50-mile site will yield the greatest remaining energy due to the shortest traveling distance needed to reach the alternate site. Failure points ranging from 20 to 75 miles were selected because failure outside of this range does not require landing at an alternate site. All three graphs in Figure 50 were calculated using Equation 18, but the alternate landing site locations vary.

$$Energy_{@alternate\ site} = Energy_{@\ failure} - Energy_{required\ to\ travel\ to\ alternate\ site} \tag{18}$$

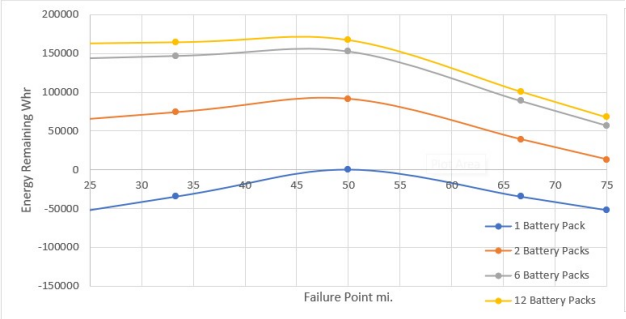

(a) Energy Remaining after Landing at 50 miles

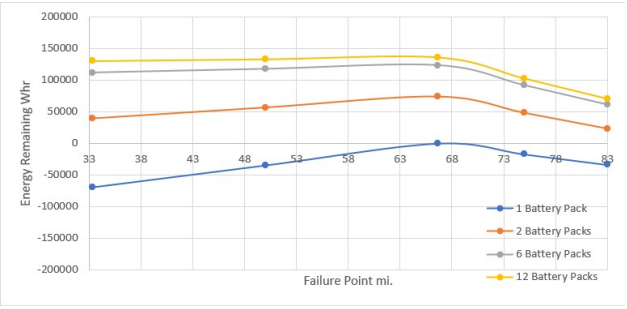

(b) Energy Remaining after Landing at 66 miles

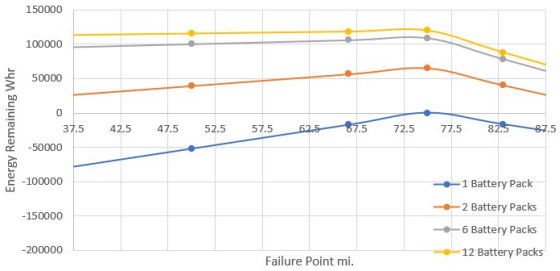

(c) Energy Remaining after Landing at 75 miles

Fig. 50 Energy Remaining after Landing at Various Alternate locations

XVI. Vehicle Cost

A. Cost Analysis

The cost analysis for the Blitzen was estimated using Wayne Johnson's NASA Design and Analysis of Rotorcraft (NDARC) [25] and cost analysis on eVTOL aircraft from the Airbus A^3 air taxi analytic framework article [26].

1. Battery/Replacement Cost

The average cost for the battery is $132 per kWh [27],and with this data, the entire battery cost is $38000. However, this is not a fixed cost due to the volatility of the material price for the battery. The battery has 6 packs, and each pack costs $6400, excluding labor and extra equipment costs.

2. Total Cost Calculation

The total cost was estimated using the Scott Rotorcraft Cost Model from NDARC. The component costs were calculated using the fully-parametric equations and vehicle parameters. Equations relied on vehicle geometry, GTOW, and expected commercialization with the production of 500 units. Moreover, integration and assembly costs and expected profit were factored in to total cost estimation. Motors, batteries, and motor controllers costs were added to the total cost from manufacturer datasheets, as the Scott Rotorcraft Model only includes turbine engine powerplant cost estimates. Due to the fact that this aircraft will be widely used in the commercial sector and is a not an experimental one-off, the total purchase cost is an important factor considered during the design process. Blitzen's total purchase price will be $1,926,700.

3. Charging Cost

The cost for the charging the battery from 0% to 100% uses the U.S. average commercial electricity cost per kWh of $0.12 and total energy required for the mission, and the cost per charging comes out to be $35.

Table 17 Cost Breakdown

Component	Parameter
C_{Rotors}	$538,300
C_{Wing}	$213,000
$C_{Fuselage}$	$444,100
$C_{Motors\ and\ Controllers}$	$79,600
$C_{Transmission}$	$10,900
$C_{Avionics}$	$35,300
$C_{Empennage}$	$93,000
$C_{Furnishings}$	$53,300
$C_{Battery}$	$37,900
$C_{Controls\ and\ Instruments}$	$35,900
$C_{Total\ Aircraft\ components}$	$1,541,300
$C_{Manufacturing\ and\ Profit}$	$385,400
$C_{Total\ Purchase\ Cost}$	$1,926,700

XVII. Weight Breakdown

Table 18 Blitzen Weight Breakdown

Item	Weight (kg)	Weight (lb)
Aerodynamics Group		
MR Blades	171.8	378.8
Rotorprop Blades	10.8	23.8
Wing	77.0	169.7
Vertical Stabilizer	57.8	127.4
Horizontal Stabilizer	27.3	60.3
Fuselage Group		
Skid Landing Gear	82.0	180.8
Exterior Skin	38.3	84.6
Floor and Walls	86.6	191.0
Airframe Structure	237.1	522.8
Motors Group		
MR Motors	120.0	264.6
MR Motor Controllers	40.8	90.0
Rotorprop Motors	48	105.8
Rotorprop Motor Controllers	27.2	60.0
Swivel Mechanism Motors	10.6	23.4
Propulsion Group		
MR Gearbox	81.8	180.4
MR Hub	52.7	116.2
MR Fairing	13.7	30.1
Rotorprop Gearbox	22.5	49.6
Rotorprop Hub	13.2	29.1
Rotorprop Spinner	1.1	2.5
Furnishing and Equipment Group		
Pilot Seat	13.6	30
Passenger Seats	36.3	80
Miscellaneous		
Batteries	719.1	1585.7
Flight Control	7.5	16.5
Instruments	7.5	16.5
Avionics	30	66.2
Load and Handling		
Pilot	81.6	180
Passengers Control	326.5	720
Baggage	150.6	332
Total	**2593**	**5717.8**

XVIII. Summary

In response to the RFP for the 2021-2022 VFS Student Design Competition, sponsored by Bell Helicopter, the University of Maryland undergraduate team presents the Blitzen. Blitzen bolts through city skies at 130 knots using its fully electric propulsion system. It safely and efficiently ferries passengers, with special consideration for people with disabilities, and provides them a luxury and speedy form of transportation. It quietly cruises with its large wing and rotorprop in pusher configuration, efficiently conducting its role as an air taxi while handily exceeding the required 100 mile radius. The configuration is a Lift and Thrust Compound SMR, and is designed to charge into the electrifying future of eVTOLs, while using the time tested and proven single main rotor design as the backbone for its design.

Not only is Blitzen feature-packed with innovative and cutting-edge technologies, but it is also structurally sound and designed with safety in mind for every component. All electrical and propulsion systems have redundancies to prevent single point failures. The large composite main rotor allows for auto rotation in an event of emergency. The Blitzen is easily re configurable and has the potential to be a standard use eVTOL aircraft with many applications, such as a delivery vehicle, emergency evacuation (MEDVAC), and combat search and rescue (CSAR). It is easy to see the growth potential and the need for eVTOLs in today's environmentally driven and fast-paced society, and equally easy to see that as lightning graces the sky now, Blitzen will soon follow.

Fig. 51 Blitzen Night Flight over Washington, DC

Fig. 52 Blitzen Landed on a Helipad

References

[1] Smialowski, B., "Tesla's Musk hints of battery capacity jump ahead of industry event," , 2020. URL https://www.reuters.com/article/us-tesla-batteries/teslas-musk-hints-of-battery-capacity-jump-ahead-of-industry-event-idUSKBN25L0MC.

[2] Kliever, A., "Sion Power Demonstrates More Than 2500 Cycles in Licerion® Rechargeable Battery Technology," *Sion Power*, 2022. URL https://sionpower.com/2022/sion-power-demonstrates-more-than-2500-cycles-in-licerion-rechargeable-battery-technology/#:~:text=Tucso%2C%20AZ%20%E2%80%94%20March%209%2C,to%2070%25%20of%20initial%20capacity.

[3] Emrax, *Manual For EMRAX Motors/ Generators*, 2020. URL https://emrax.com/wp-content/uploads/2020/03/manual_for_emrax_motors_version_5.4.pdf.

[4] Araujo, K., "Battery Cell Comparison," , 2022. URL https://www.epectec.com/batteries/cell-comparison.html.

[5] Lidbeck, A., and Syed, K. R., "Experimental Characterization of Li-ion Battery cells for Thermal Management in Heavy Duty Hybrid Applications," *Master of Science Thesis, Chalmers University of Technology*, 2017.

[6] Leishman, G. J., *Principles of Helicopter Aerodynamics*, Cambridge University Press, 2006.

[7] Nagaraj, V. T., and Chopra, I., *Preliminary Design of Rotorcraft*, Lecture Notes, ENAE 481, University of Maryland, 2020.

[8] Kadhiresan, A. R., and Duffy, M. J., "Conceptual Design and Mission Analysis for eVTOL Urban Air Mobility Flight Vehicle Configurations," *AIAA 2019 Aviation Forum*, 2019. doi:10.2514/6.2019-2873.

[9] Whiteside, S., Pollard, B., Antcliff, K., Zawodny, N., Fei, X., Silva, C., and Medina, G., "Design of a Tiltwing Concept Vehicle for Urban Air Mobility," *NASA STI Program Report Series*, 2021.

[10] Johnson, W., "A Quiet Helicopter for Air Taxi Operations," *The VFS Aeromechanics for Advanced Vertical Flight Technical Meeting*, 2020. doi:10.2514/6.2017-3442.

[11] Yeo, H., and Johnson, W., "Aeromechanics Analysis of a Heavy Lift Slowed-Rotor Compound Helicopter," *Journal of Aircraft*, Vol. 44, No. 2, 2007. doi:10.2514/1.23905.

[12] Duffy, M. J., Wakayama, S., Hupp, R., Lacy, R., and Stauffer, M., "A Study In Reducing the Cost of Vertical Flight with Electric Propulsion," *17th AIAA Aviation Technology, Integration, and Operations Conference*, 2017. doi:10.2514/6.2017-3442.

[13] Panda, B., and Chopra, I., "Dynamic Stability of Hingeless and Bearingless Rotors in Forward Flight," *Computers & Mathematics with Applications*, Vol. 12A, No. 1, 1986, pp. 111–130.

[14] Hoerner, S. F., *Fluid–Dynamic Drag*, 1965.

[15] Raymer, D. P., *Aircraft Design: A Conceptual Approach*, 2nd ed., American Institute of Aeronautics and Astronautics, Inc., 1992.

[16] Tzinis, I., "Technology Readiness Level," , 2021. URL https://www.nasa.gov/directorates/heo/scan/engineering/technology/technology_readiness_level.

[17] Scooter, D., "How long does it take to charge a Tesla?" , 2021. URL https://electrek.co/2021/11/03/how-long-does-it-take-to-charge-a-tesla/#:~:text=Here's%20a%20breakdown%20of%20the,Supercharger)%3A%2015%2D25%20minutes.

[18] Bobby, "Battery Life Cycle vs. Cycle Life," , 2014. URL https://www.upsbatterycenter.com/blog/battery-life-cycle-vs-cycle-life/#:~:text=Each%20round%20of%20full%20discharge,are%20on%20borrowed%20time!!

[19] Batir, U., "Finite Element Analysis of Landing Skid of Helicopter Using Static Load Approximation," *Istanbul Technical University*, 2014.

[20] Chen, W., Qian, X., He, X., and Liu, J., "Enhanced ultraviolet resistance of Kevlar fibers with TiO<inf>2</inf> films," 2011.

[21] Thales, *Thales Avionics for Helicopters*, 2020.

[22] I.V.A.O., "Helicopter lights," , 2022. URL https://mediawiki.ivao.aero/index.php?title=Helicopter_lights.

[23] Edwards, T., and Price, G., "eVTOL Passenger Acceptance," *NASA STI Program Report Series*, 2020.

[24] Pegg, R. J., "A Summary and Evaluation of Semi-Empirical Methods for the Prediction of Helicopter Rotor Noise," *National Aeronautics and Space Administration*, , No. NASA Technical Memorandum 80200, 1979.

[25] Johnson, W., "NDARC NASA Design and Analysis of Rotorcraft, Release 1.15," *NASA*, 2020.

[26] Sridharan, A., "Air Taxi Analytic Framework," *Acubed*, 2019.

[27] Henze, V., "Battery Pack Prices Fall to an Average of $132/kWh, But Rising Commodity Prices Start to Bite," , 2021. URL https://about.bnef.com/blog/battery-pack-prices-fall-to-an-average-of-132-kwh-but-rising-commodity-prices-start-to-bite/.